Article

Cell Reports

The Nuclear Orphan Receptor NR2F6 Is a Central Checkpoint for Cancer Immune Surveillance

Graphical Abstract

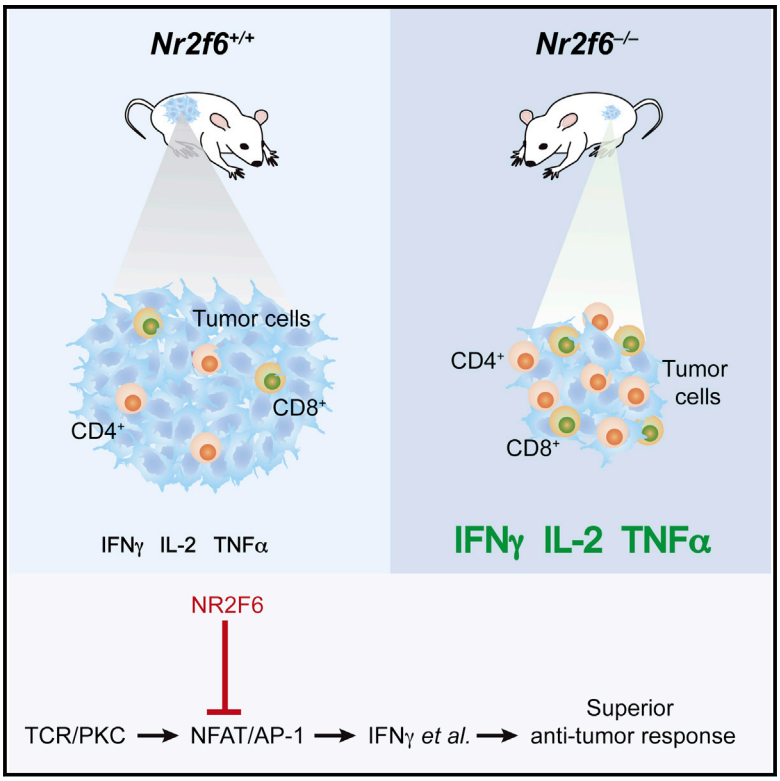

Authors

Natascha Hermann-Kleiter, Victoria Klepsch, Stephanie Wallner, ..., Thomas Gruber, Dominik Wolf, Gottfried Baier

Correspondence

natascha.kleiter@i-med.ac.at (N.H.-K.), gottfried.baier@i-med.ac.at (G.B.)

In Brief

Immune checkpoint blockade has emerged as an effective cancer immunotherapy strategy. Here, Hermann-Kleiter et al. demonstrate a role for the nuclear orphan receptor NRF26 in tumor immune surveillance, effectively identifying an intracellular immune checkpoint in effector T cells that governs the amplitude of anti-cancer immunity.

Highlights

- Genetic ablation of *Nr2f6* induces immune-mediated cancer surveillance
- *Nr2f6*$^{-/-}$ mice display an immune contexture favoring anti-tumor responses
- NR2F6 represses transcription of key cytokines in CD4^{+} and CD8^{+} effector T cells
- NR2F6 controls the amplitude of tumor immunity

Hermann-Kleiter et al., 2015, Cell Reports *12*, 2072–2085
September 29, 2015
http://dx.doi.org/10.1016/j.celrep.2015.08.035

OPEN ACCESS
CellPress

Cell Reports
Article

The Nuclear Orphan Receptor NR2F6 Is a Central Checkpoint for Cancer Immune Surveillance

Natascha Hermann-Kleiter,[1,5,*] Victoria Klepsch,[1,5] Stephanie Wallner,[2] Kerstin Siegmund,[1] Sebastian Klepsch,[1] Selma Tuzlak,[3] Andreas Villunger,[3] Sandra Kaminski,[1] Christa Pfeifhofer-Obermair,[1] Thomas Gruber,[1] Dominik Wolf,[2,4] and Gottfried Baier[1,*]

[1]Translational Cell Genetics, Department for Pharmacology and Genetics, Medical University of Innsbruck, 6020 Innsbruck, Austria
[2]Laboratory of Tumor Immunology, Tyrolean Cancer Institute & Internal Medicine V, Medical University of Innsbruck, 6020 Innsbruck, Austria
[3]Division of Developmental Immunology, Medical University of Innsbruck, 6020 Innsbruck, Austria
[4]Medical Clinic III, Oncology, Hematology & Rheumatology, University Clinic Bonn, 53127 Bonn, Germany
[5]Co-first author
*Correspondence: natascha.kleiter@i-med.ac.at (N.H.-K.), gottfried.baier@i-med.ac.at (G.B.)
http://dx.doi.org/10.1016/j.celrep.2015.08.035

SUMMARY

Nuclear receptor subfamily 2, group F, member 6 (NR2F6) is an orphan member of the nuclear receptor superfamily. Here, we show that genetic ablation of *Nr2f6* significantly improves survival in the murine transgenic TRAMP prostate cancer model. Furthermore, *Nr2f6*$^{-/-}$ mice spontaneously reject implanted tumors and develop host-protective immunological memory against tumor rechallenge. This is paralleled by increased frequencies of both CD4$^+$ and CD8$^+$ T cells and higher expression levels of interleukin 2 and interferon γ at the tumor site. Mechanistically, CD4$^+$ and CD8$^+$ T cell-intrinsic NR2F6 acts as a direct repressor of the NFAT/AP-1 complex on both the *interleukin 2* and the *interferon γ* cytokine promoters, attenuating their transcriptional thresholds. Adoptive transfer of *Nr2f6*-deficient T cells into tumor-bearing immunocompetent mice is sufficient to delay tumor outgrowth. Altogether, this defines NR2F6 as an intracellular immune checkpoint in effector T cells, governing the amplitude of anti-cancer immunity.

INTRODUCTION

Adaptive immunity together with innate effector immune cells is established to efficiently control malignant cells. The importance of T cells for tumor cell elimination is underscored by the observation that tumor infiltration by T cells represents a valuable prognostic marker in different human cancer types (Hunder et al., 2008; Hodi et al., 2010; reviewed in Motz and Coukos, 2013). Residual T cell reactivity against malignant cells is limited by various components of immune evasion, such as local accumulation of immunosuppressive cell types within the tumor microenvironment. Together this favors tumor escape from the immune system instead of immune-mediated cancer cell elimination (for review, see Zitvogel et al., 2006; Zou, 2005; Motz and Coukos, 2013). Consistently, interleukin 2 (IL-2) and interferon γ (IFN-γ) are both additional key prognostic indicators mirroring a protective anti-tumor immune response in humans. High IL-2 levels thereby favor CD8$^+$ T cell effector functions (Pipkin et al., 2010). High IFN-γ directly modulates both cancer biology (e.g., by inducing tumor cell senescence) (Schwartzentruber et al., 2011; Bedognetti et al., 2013; Braumüller et al., 2013; Galon et al., 2013) and induces an immune contexture favoring continuous tumor cell elimination, a concept coined "cancer immune surveillance" (Shankaran et al., 2001).

Manipulating the immune system to harness anti-tumor immune responses for the treatment of cancer patients has been a major goal for many decades. Promising novel therapeutic advances blocking immune system inhibitory pathways, such as cytotoxic T lymphocyte-associated protein 4 (CTLA-4) and programmed cell death 1 (PD-1)/PD-1 ligand (PD-L1), are referred to as "immune checkpoints" (i.e., inhibitory signaling intermediates that control the duration and amplitude of physiological immune responses) are successful entering into clinics (Hodi et al., 2010; Brahmer et al., 2010; Robert et al., 2011; Hamid et al., 2013; Topalian et al., 2012; Powles et al., 2014; Tumeh et al., 2014; Gubin et al., 2014). In addition, adoptive T cell transfer therapy or vaccination approaches are now also providing more encouraging results, especially when combined with cytokines or the above mentioned immune checkpoint-antagonizing antibodies (van den Eertwegh et al., 2012; Kalos and June, 2013; Restifo et al., 2012; Kantoff et al., 2010; Bodor et al., 2012; Motz and Coukos, 2013; Schwartzentruber et al., 2011). Even though these approaches are exciting, there is an unmet medical need, as still only a limited number of patients response to and even less patients are potentially cured by these approaches. Thus, there is a high scientific interest to explore novel cancer immunotherapeutic approaches with the ultimate goal to further strengthen the patient's immune system.

Notably, mechanistic processes that support immune-mediated tissue destruction appear to be strikingly analogous in

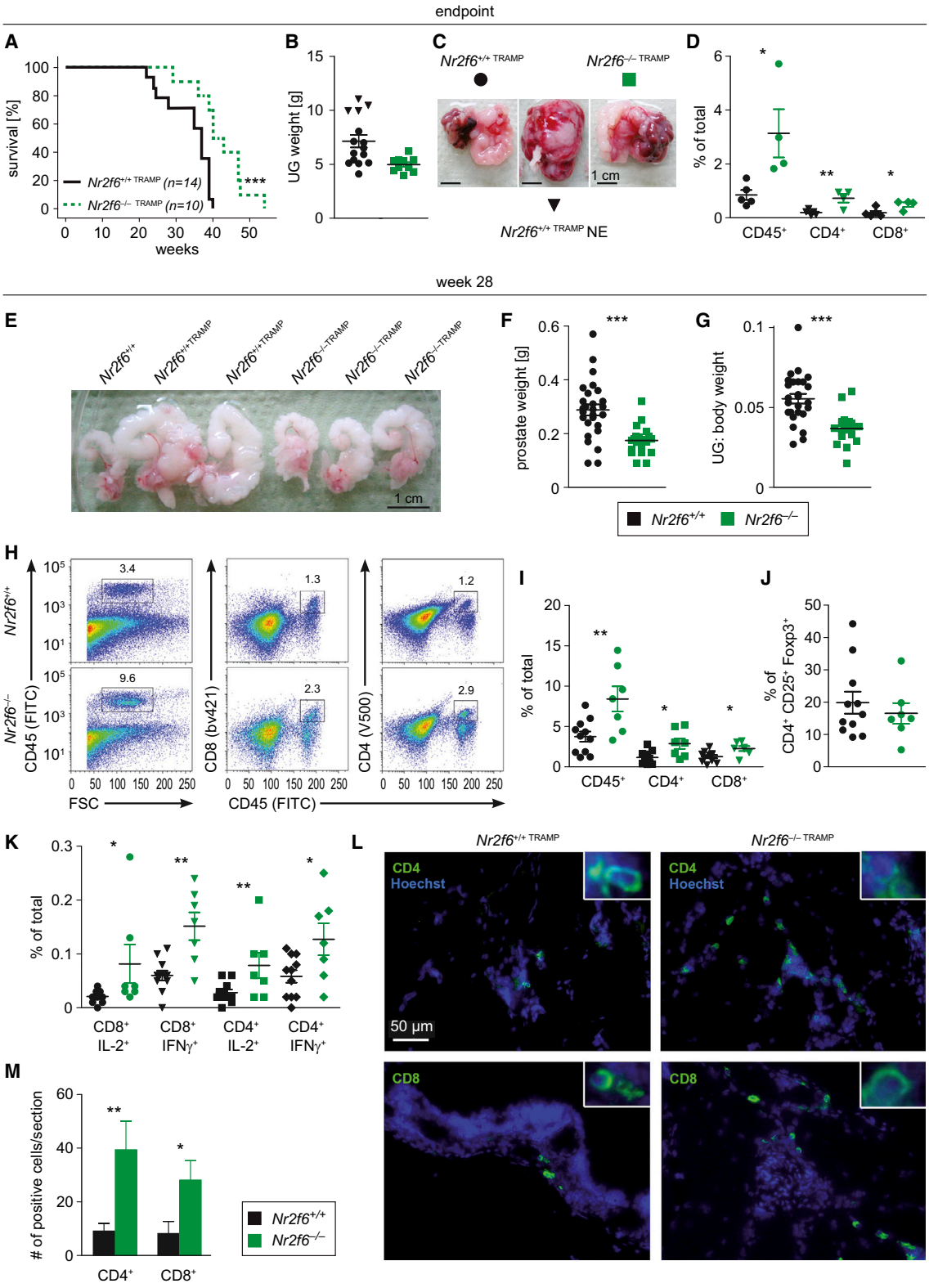

(legend on next page)

autoimmunity and cancer. We previously demonstrated that the nuclear receptor subfamily 2, group F, member 6 (NR2F6; also called COUP-TFIII or Ear2) represents an important gatekeeper of antigen receptor-induced cytokine response thresholds of pro-inflammatory $CD4^+$ Th17 lymphocytes (Hermann-Kleiter et al., 2008). In these autoimmunity-promoting Th17 cells, NR2F6 directly antagonizes the binding of the transcription factors NFAT and, particularly, retinoic acid receptor-related orphan receptor-γ-t (RORc) to the *Il17* cytokine locus (Hermann-Kleiter et al., 2012), thereby reducing central nervous system inflammation. Here, we employed various types of transplantable and spontaneous tumor models to define the role of NR2F6 in tumor immunology. Using these model systems, we provide strong experimental evidence that genetic deletion of *Nr2f6* is both necessary and sufficient to induce host-protective immune rejection of cancer. *Nr2f6* deficiency leads to augmented intratumoral effector $CD4^+$ and $CD8^+$ T cell infiltration and strongly enhances local production of IL-2, IFN-γ, and tumor necrosis factor-α (TNF-α), thereby forming an immune environment that allows strong anti-tumor T cell responses in tumor-bearing mice.

RESULTS

Loss of NR2F6 Prolongs Survival of TRAMP Mice, an Autochthonous Model of Prostate Cancer

We employed the murine transgenic adenocarcinoma of the mouse prostate (TRAMP) model, in which prostate-specific expression of SV40 large T antigen results in prostate cancer (Greenberg et al., 1995), to evaluate the role of NR2F6 in cancer immunity. Male TRAMP mice with different *Nr2f6* genotypes ($Nr2f6^{+/+TRAMP}$ and $Nr2f6^{-/-TRAMP}$) were analyzed at week 22 and 28, as well as when terminally ill. While all $Nr2f6^{+/+TRAMP}$ mice had to be sacrificed due to high tumor burden latest at week 40, 50% of $Nr2f6^{-/-TRAMP}$ mice remained alive at this time point (Figure 1A). The majority of the primary tumor masses were composed of atypical epithelial hyperplasia (AH); however, 26% of $Nr2f6^{+/+TRAMP}$ mice developed aggressive neuroendocrine (NE) tumors, as identified through histomorphological analysis (Figures 1B and 1C). In contrast to $Nr2f6^{+/+TRAMP}$ mice and despite a similar prostate tumor incidence, we never observed any NE differentiation in tumors from $Nr2f6^{-/-TRAMP}$ mice. Although tumor growth was significantly delayed in $Nr2f6^{-/-TRAMP}$ mice, all animals had to be sacrificed at week 55. Endpoint analyses indicated an enhanced number of intratumoral $CD45^+$, $CD4^+$, and $CD8^+$ immune cells in $Nr2f6^{-/-TRAMP}$ mice (Figure 1D).

In order to define the mechanism underlying the observed survival benefit due to delayed tumor outgrowth in $Nr2f6^{-/-TRAMP}$ mice, we next analyzed in detail prostate tumors at pre-defined time points. At week 28, tumor burden (quantified by calculating urogenital tract weight without the bladder and prostate relative to the total body weight) was significantly reduced in $Nr2f6^{-/-TRAMP}$ compared to $Nr2f6^{+/+TRAMP}$ mice (Figures 1E–1G); notably, no differences in overall body weight could be detected at any time point (Figures S1A–S1C). At week 28, we observed significantly more prostate tumor-infiltrating $CD4^+$ and $CD8^+$ T cells in $Nr2f6^{-/-TRAMP}$ mice than in $Nr2f6^{+/+TRAMP}$ mice (Figures 1H and 1I), whereas comparable numbers of $CD4^+CD25^+Foxp3^+$ tumor-infiltrating regulatory T cells could be detected in the two genotypes (Figure 1J). Tumor-infiltrating immune cells contained increased frequencies of $CD8^+IL\text{-}2^+$, $CD8^+IFN\text{-}\gamma^+$, $CD4^+IL\text{-}2^+$, and $CD4^+IFN\text{-}\gamma^+$ T lymphocytes in

Figure 1. Loss of NR2F6 Prolongs Survival in the Autochthonous Prostate Cancer Model TRAMP Due to Enhanced Numbers of Cytokine-Secreting Infiltrating T Cells

(A) Endpoint analysis of male $Nr2f6^{+/+TRAMP}$ (n = 14) and $Nr2f6^{-/-TRAMP}$ (n = 10) mice (A) showed a significant survival benefit in $Nr2f6^{-/-TRAMP}$ mice depicted by a Kaplan-Meier curve and statistics analyzed by the log-rank test (p = 0.0018).

(B) Weight of TRAMP urogenital (UG) tract at endpoint was not significantly different between $Nr2f6^{+/+TRAMP}$ and $Nr2f6^{-/-TRAMP}$ mice. Aggressive neuroendocrine (NE) tumors in wild-type mice shown in triangles were absent in the *Nr2f6*-deficient cohort.

(C) One representative endpoint TRAMP prostate tumor with seminal vesicle metastasis derived from $Nr2f6^{+/+TRAMP}$ (circle, black) and $Nr2f6^{-/-TRAMP}$ (square, green) mice is shown as well as one $Nr2f6^{+/+TRAMP}$ NE tumor (triangle, black).

(D) Phenotypic characterization of $CD45^+$ TILs in $Nr2f6^{+/+TRAMP}$ (black) or $Nr2f6^{-/-TRAMP}$ (green) of prostate tumors taken at the endpoint of the experiment: higher cell percentages of total infiltrating immune cells expressing $CD45^+$ (p = 0.02), $CD45^+CD4^+$ (p = 0.009), or $CD45^+CD8^+$ (p = 0.03) are detected in $Nr2f6^{-/-TRAMP}$ despite comparable tumor sizes.

(E) Gross examination of urogenital tracts at week 28 of $Nr2f6^{+/+TRAMP}$ and $Nr2f6^{-/-TRAMP}$ mice.

(F and G) (F) Significantly decreased UG tracts relative to body weight (p < 0.0001) and (G) prostate weight (p < 0.0001) were observed in $Nr2f6^{-/-TRAMP}$ mice (n = 21) when compared to $Nr2f6^{+/+TRAMP}$ mice (n = 27). Four prostate tumors within both cohorts were excluded from statistical analysis at this time point as classified as outliers due to being either too small (<0.09 g) or too large (>0.5 g).

(H) Tumor single-cell suspensions isolated from $Nr2f6^{+/+TRAMP}$ or $Nr2f6^{-/-TRAMP}$ mice were analyzed by flow cytometry. The percentage of positively stained cells among total viable cells after gating on forward and side scatter is shown. Representative dot plots of prostate tumor-infiltrating $CD45^+$ single-positive and $CD45^+CD8^+$, or $CD45^+CD4^+$ double-positive T cells isolated from $Nr2f6^{+/+TRAMP}$ or $Nr2f6^{-/-TRAMP}$ mice are depicted. Numbers adjacent to outlined areas indicate the percentage of positive cells relative to parental gate.

(I) Percentage of TILs at week 28 of $Nr2f6^{+/+TRAMP}$ (n = 11) and $Nr2f6^{-/-TRAMP}$ (n = 7) mice revealed enhanced numbers of $CD45^+$ (p = 0.006), $CD45^+CD8^+$ (p = 0.002) and $CD45^+CD4^+$ (p = 0.001) cells.

(J) Equal numbers of prostate tumor-infiltrating Treg cells ($CD4^+CD25^+Foxp3^+$) in $Nr2f6^{+/+TRAMP}$ (n = 11) and $Nr2f6^{-/-TRAMP}$ (n = 7) prostate tumors.

(K) Percentages of total cytokine producing TILs within $Nr2f6^{+/+TRAMP}$ (n = 11) and $Nr2f6^{-/-TRAMP}$ (n = 7) prostate tumors: significantly enhanced numbers of $CD8^+IL\text{-}2^+$ (p = 0.049), $CD8^+IFN\text{-}\gamma^+$ (p = 0.001), $CD4^+IL\text{-}2^+$ (p = 0.002), and $CD4^+IFN\text{-}\gamma^+$ (p = 0.02) cells were found within $Nr2f6^{-/-TRAMP}$ prostate tumors.

(L) Representative cryosection of $Nr2f6^{+/+TRAMP}$ or $Nr2f6^{-/-TRAMP}$ prostate tumors immune-fluorescence staining for the T cell markers CD4 and CD8 in green and Hoechst nuclear stain in blue, respectively. Scale bar, 50 μm.

(M) Graphical representation of increased $CD4^+$ (p = 0.01) and $CD8^+$ (p = 0.03) T cell tumor infiltration in $Nr2f6^{-/-}$ mice, averaged from three fields per mouse and four mice per genotype. Error bars represent SEM and asterisk (*) indicates statistically significant differences between $Nr2f6^{+/+TRAMP}$ or $Nr2f6^{-/-TRAMP}$ tumors, as calculated using Student's t test.

Nr2f6$^{-/-TRAMP}$ mice versus *Nr2f6*$^{+/+TRAMP}$ mice (Figure 1K). Analysis by immunohistochemistry in tumors with comparable sizes confirmed significantly higher numbers of intratumoral CD4$^+$ and CD8$^+$ T cells in *Nr2f6*$^{-/-TRAMP}$ mice (Figures 1L and 1M). To address the role of NR2F6 in T cells within the tumor draining lymph node (dLN), we evaluated T cell frequency, activation status, and cytokine production at week 28. Again, the proportions of T cells that were CD45$^+$, CD4$^+$, CD8$^+$, CD44$^+$, or IFN-γ^+ were significantly elevated (Figures S1D–S1G). Even though we detected a trend toward higher intratumoral numbers of CD4$^+$RORc$^+$ and $\gamma\delta$TCR$^+$ cells in *Nr2f6*$^{-/-TRAMP}$ mice versus *Nr2f6*$^{+/+TRAMP}$ mice, the differences between the two genotypes did not reach statistical significance (Figure S1H). Similarly, we also observed a tendency toward larger proportions of CD4$^+$IL-17$^+$, CD8$^+$Tbet$^+$, DX5$^+$, and $\gamma\delta$TCR$^+$ cells that also did not reach statistical significance (Figure S1I). The same readouts were used to analyze the immune cell composition of prostate tumors and dLNs at earlier time points (i.e., at week 22). Again, reduced urogenital tract (UG) sizes in *Nr2f6*$^{-/-TRAMP}$ mice were paralleled by increased numbers of CD45$^+$ immune cells infiltrating prostate tumors, and elevated numbers of CD4$^+$IL-2$^+$ T cells in the dLNs of *Nr2f6*$^{-/-TRAMP}$ mice (Figures S1J–S1M).

Taken together, these data show that the numbers of T cells in *Nr2f6*$^{-/-TRAMP}$ tumor-bearing mice are increased both within the dLNs and at the tumor site at all three time points investigated. The enhanced production rates of IL-2 and IFN-γ may contribute to a local immune-activated microenvironment, which, in turn, significantly contributes to immune-mediated cancer growth control leading to increased survival of *Nr2f6*$^{-/-TRAMP}$ mice.

Anti-tumor Immune Response in *Nr2f6*-Deficient Mice

At this point, we were not able to exclude that loss of *Nr2f6* function in non-immune cells (for example, in prostate epithelial cells within the autochthonous TRAMP tumor model) may be causally involved in the observed alterations of tumor progression. Therefore, we next used four different highly tumorigenic cancer cell lines (TRAMP-C1, B16-OVA, B16-F10, and EG7) to analyze animal survival, tumor growth, and the tumor/dLN immune microenvironment; of note, all four lines are genetically wild-type for *Nr2f6*. Similar to the findings from the autochthonous TRAMP model, survival in *Nr2f6*-deficient mice receiving *Nr2f6* wild-type tumor cell lines was significantly enhanced. Figures 2A and 2B demonstrate the delayed growth kinetics of subcutaneously injected TRAMP-C1 and B16-OVA tumors in *Nr2f6*-deficient mice. TCRVβ repertoire of wild-type and *Nr2f6*-deficient T lymphocytes prior or post-B16-OVA tumor challenge from naive or tumor dLN was investigated via clonality analysis of the individual Vβ gene families of the CDR3 region. These data indicated unaltered clonal composition of the T cell compartment between wild-type and *Nr2f6*-deficient T cells in tumor-bearing mice (Figures S2A and S2B). Furthermore, 75% of *Nr2f6*$^{-/-}$ mice injected with the EG7 lymphoma cell line completely rejected EG7 tumors and remained tumor-free throughout the entire 10-month experimental period; in contrast, all *Nr2f6*$^{+/+}$ mice challenged with EG7 cells had to be sacrificed as early as day 21 post-injection because of their high tumor burden (Figures 2C and 2D).

Of note, comparing genetic NR2F6 deletion with blocking interaction of PD-1 with its ligand PD-L1 provides evidence that the observed superior anti-tumor immunity in *Nr2f6*$^{-/-}$ mice is well comparable to the benefit of PD-L1 blocking therapy in wild-type mice (employing the established protocol with neutralizing Ab10F.9G2; Gros et al., 2014). This suggests that NR2F6 and the PD-1/PD-L1 axis control cancer immunity to a similar extent (Figure 2E).

As next step the B16-OVA subcutaneous (s.c.) tumor model was used for an extensive analysis of tumor-infiltrating immune cells at day 14 after tumor cell injection (Figure 3A), employing a stratified CD45$^+$/CD3$^+$/CD4$^+$ or CD8$^+$ gating strategy (as outlined in Figures S3A and S3B). As in the autochthonous model of prostate cancer, B16-OVA tumors grown in *Nr2f6*$^{-/-}$ mice exhibited significantly increased numbers of tumor-infiltrating CD45$^+$CD3$^+$CD4$^+$ and CD45$^+$CD3$^+$CD8$^+$ T cells, calculated at the level of total numbers on a weight (i.e., gram) basis when compared to wild-type mice (Figures 3B and 3C). This particular phenotype of *Nr2f6*$^{-/-}$ mice was independent of the B16-OVA tumor size (Figure S3C). Analysis in tumors with comparable sizes by immunohistochemistry confirmed the markedly enhanced intratumoral CD4$^+$ and CD8$^+$ T cell numbers in *Nr2f6*$^{-/-}$ mice (Figures S3D and S3E), well reflecting relative levels of tumor-infiltrating lymphocytes (TILs) (i.e., percentage of CD45$^+$, CD45$^+$CD3$^+$, CD45$^+$CD8$^+$, or CD45$^+$CD4$^+$cells; Figure S3F). Pronounced CD8$^+$ and CD4$^+$ T cell effector functions in *Nr2f6*$^{-/-}$ mice were found to be associated with markedly higher expression of CD25 and PD-1 on both T cell subsets when compared to wild-type animals (Figures 3D and 3E).

Because immunosuppressive immune cells such as Tregs, tumor-associated macrophages (TAM), and myeloid-derived suppressor cells (MDSCs) in the tumor microenvironment are established to promote T cell dysfunction and reduction of these cells would at least in part explain increased anti-tumor immune responses in *Nr2f6*$^{-/-}$ mice, we evaluated the extend of tumor infiltration by Treg, MDSC, and TAM (Figures 3D and 3F). In *Nr2f6*$^{-/-}$ mice, we could not detect any reduction of Treg accumulation but could even observe an increased abundance of these cells in B16-OVA tumor tissues of *Nr2f6*$^{-/-}$ mice. Nevertheless, the clearly increased numbers of CD4$^+$ and CD8$^+$ effector TILs in *Nr2f6*$^{-/-}$ mice outweigh this increase of immunosuppressive cell types, as the intratumoral ratios of Teff/Treg did not show a significant difference between mice of both genotypes. The ratio of CD8$^+$ and CD4$^+$ effector T cells to either MDSC or TAM remain even in favor of the effector cell populations in *Nr2f6*$^{-/-}$ mice.

In tumor-bearing *Nr2f6*$^{-/-}$ mice, CD4$^+$ and CD8$^+$ tumor-infiltrating T cell subsets expressed significantly increased amounts of IL-2, IFN-γ, and TNF-α (Figures 4A–4C). Among the dLN-derived cells, CD4$^+$ T cells producing IL-2 and IFN-γ as well as CD8$^+$ T cells secreting IFN-γ were significantly more abundant in *Nr2f6*$^{-/-}$ mice (Figures S4A–S4C) as were activated CD4$^+$ and CD8$^+$ T cells (CD4$^+$CD44^{hi}; CD8$^+$CD44^{hi}) (Figure S4D). Notably, we could not detect any obvious alterations in tumor-infiltrating natural killer (NK) cells (DX5$^+$), macrophages (CD11b$^+$), or DC subsets (CD11c$^+$CD11b$^+$ and CD11c$^+$CD8a$^+$) in *Nr2f6*$^{-/-}$ compared to wild-type tumor-bearing mice (Figure S4E).

Next, the functional importance of increased cytokine secretion by *Nr2f6*$^{-/-}$ T cells was investigated by blocking IL-2 and IFN-γ function using systemic injection of antagonizing

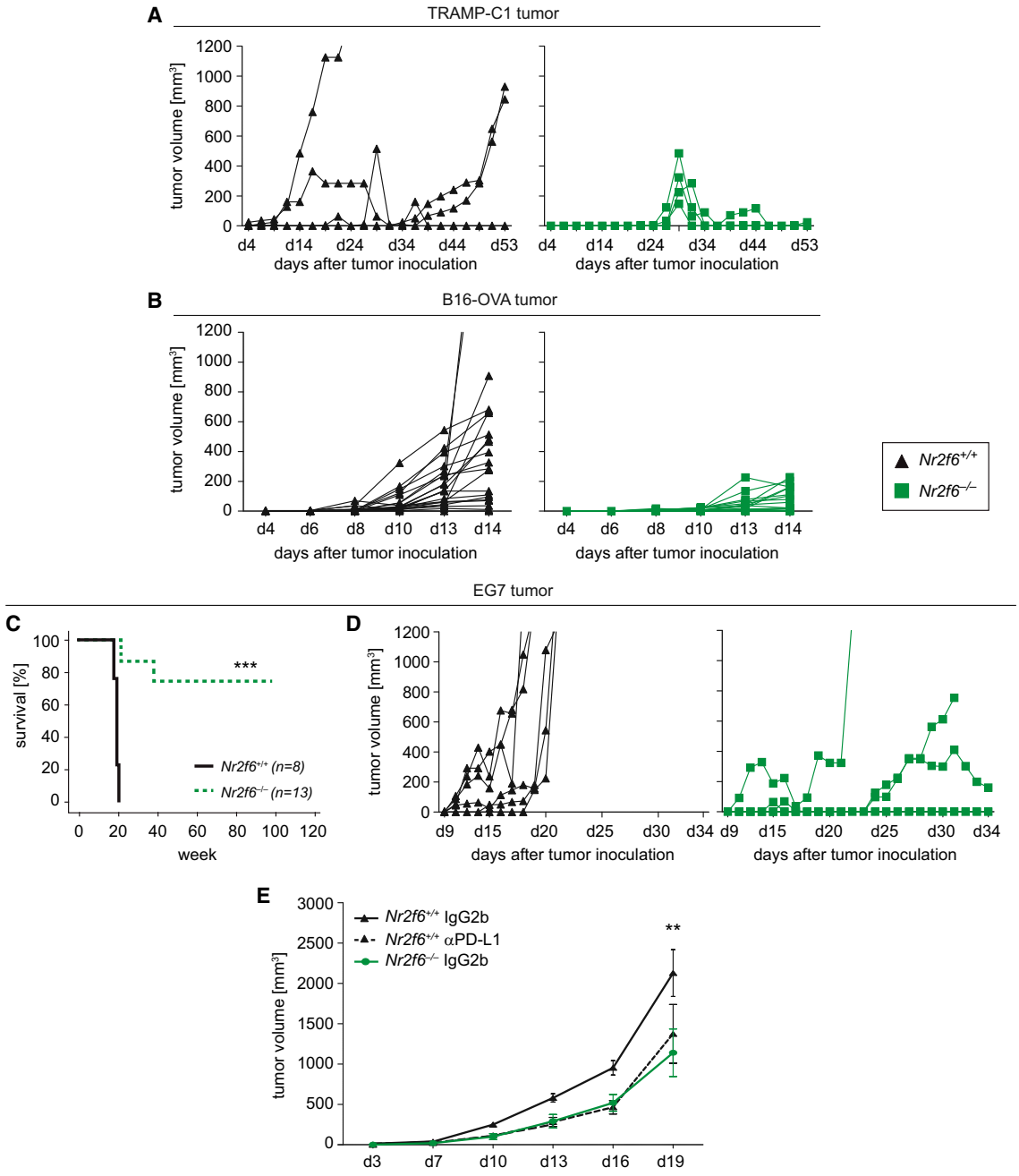

Figure 2. *Nr2f6*$^{-/-}$ Mice Reject Transplantable Subcutaneous Tumors

The kinetics of tumor cell growth in 8- to 12-week-old *Nr2f6*$^{+/+}$ (black) and *Nr2f6*$^{-/-}$ (green) mice bearing subcutaneously TRAMP-C1 prostate tumor cells, B16-OVA melanoma, or EG7 lymphoma.

(A) Tumor growth curve of 1 × 10^6 TRAMP-C1 cells inoculated into *Nr2f6*$^{+/+}$ (n = 5) and *Nr2f6*$^{-/-}$ (n = 5) mice (ANOVA, $p < 0.0001$).

(B) Kinetics of 1 × 10^5 (n = 5) B16-OVA cells in *Nr2f6*$^{+/+}$ (n = 17) and *Nr2f6*$^{-/-}$ (n = 17) mice, which were used for subsequent analysis (ANOVA, $p = 0.0017$).

(C) Significant survival benefit in *Nr2f6*$^{-/-}$ (n = 8) compared to *Nr2f6*$^{+/+}$ (n = 13) mice injected with 1.5 × 10^5 EG7 tumor cells shown by a Kaplan-Meier curve, statistically analyzed by a log-rank test ($p = 0.0001$).

(D) Kinetics of EG7 tumor cell growth in *Nr2f6*$^{+/+}$ (n = 5) and *Nr2f6*$^{-/-}$ (n = 5) mice (ANOVA, $p < 0.0001$). Results shown are derived from at least two independent experiments.

(E) Tumor growth curve in *Nr2f6*$^{+/+}$ mice (n = 9) injected s.c. with 5 × 10^5 B16-OVA cells and administered i.p. with 0.5 mg of an anti-mouse PD-L1 blocking antibody as immune checkpoint inhibitor is comparable to tumor growth curve seen in *Nr2f6*$^{-/-}$ mice (n = 8) injected with rat immunoglobulin G (IgG) control alone. Summary of three independent experiments is shown, and data are expressed as the mean ± SEM, IgG control in wild-type recipients versus anti-mouse PD-L1 blocking antibody ($p = 0.0019$) statistically analyzed by two-way ANOVA.

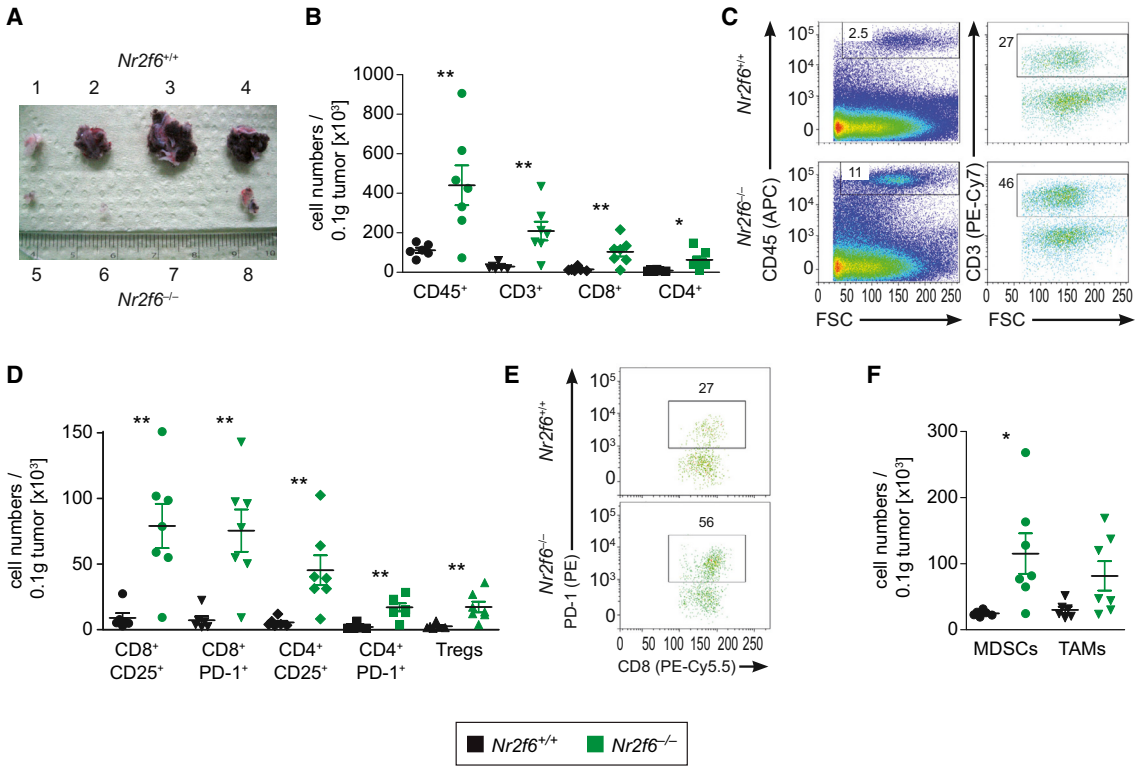

Figure 3. Enhanced Numbers of Tumor-Infiltrating T Cells in *Nr2f6*-Deficient Mice Bearing B16-OVA Transplantable Melanomas

(A) Gross examination of B16-OVA melanomas from *Nr2f6*$^{+/+}$ (top) and *Nr2f6*$^{-/-}$ (bottom) mice 14 days after subcutaneous injection of 1 × 10^5 tumor cells.

(B) Tabulation of *Nr2f6*$^{+/+}$ (n = 6) and *Nr2f6*$^{-/-}$ (n = 7) B16-OVA tumor-infiltrating cells on day 14. Significantly increased absolute cell numbers of CD45$^+$ (p = 0.01), CD3$^+$ (p = 0.05), CD8$^+$ (p = 0.007), and CD4$^+$ (p = 0.015) per 0.1 g of tumor tissue were detected in *Nr2f6*$^{-/-}$ mice.

(C) Dot plots of B16-OVA tumor-infiltrating CD45$^+$ and CD3$^+$ cells derived from *Nr2f6*$^{+/+}$ and *Nr2f6*$^{-/-}$ tumor-bearing mice (for detailed gating strategy, see Figure S3).

(D) Immune cell characterization of *Nr2f6*$^{+/+}$ (n = 6) and *Nr2f6*$^{-/-}$ (n = 7) B16-OVA tumor-infiltrating cells per 0.1 g of tumor tissue, gated on CD45$^+$CD3$^+$ positive cells did reveal increased absolute cell numbers of CD8$^+$CD25$^+$ (p = 0.003); CD8$^+$PD-1$^+$ (p = 0.003); CD4$^+$CD25$^+$ (p = 0.008); CD4$^+$PD-1$^+$ (p = 0.001); and CD4$^+$CD25$^+$Foxp3$^+$ Treg cells (p = 0.007).

(E) Dot plots of B16-OVA tumor-infiltrating CD8$^+$PD-1$^+$ cells derived from *Nr2f6*$^{+/+}$ and *Nr2f6*$^{-/-}$ mice.

(F) Significantly increased absolute cell numbers of CD11b$^+$Gr-1$^+$ myeloid derived suppressor cells (p = 0.02), and a trend for tumor associated macrophages (p = 0.06) (CD11b$^+$F/80$^+$) could be detected in tumors of *Nr2f6*$^{-/-}$ (n = 7) mice.

antibodies into tumor-bearing mice in vivo. These experiments identified IFN-γ as key effector cytokine at least in part explaining enhanced anti-tumor immunity of *Nr2f6*$^{-/-}$ mice, as anti-IFN-γ antibodies abrogated the tumor-protective phenotype of *Nr2f6*$^{-/-}$ animals (Figure 4D). Increased cytokine production appears to be particularly linked to tumor challenge, as we could not detect an enhanced steady-state cytokine-production potential of CD4$^+$ or CD8$^+$ T cells in tumor-free *Nr2f6*$^{-/-}$ mice (Figure S5A).

The impact of *Nr2f6* deficiency on tumor metastasis was next evaluated by challenging each mouse genotype with intravenously (i.v.) administered B16-F10 cells, which are known to form lung metastases upon i.v. injection. Similar to our previous data, formation of lung metastases was significantly reduced at day 14 and 19 post-injection, as quantified by reduction of the number of tumor foci in the lungs of *Nr2f6*-deficient mice (Figures 5A and 5B). Thus, deficiency of *Nr2f6* in non-cancer cells appears to strongly enhance the anti-metastatic activity of the immune system.

To evaluate in detail whether *Nr2f6*-deficiency also allows induction of immunological memory, we re-challenged *Nr2f6*$^{-/-}$ mice that had previously rejected EG7 tumor cells (termed "memory *Nr2f6*$^{-/-}$ mice") in parallel to 10-month-old sex-matched EG7 tumor antigen-naive *Nr2f6*$^{+/+}$ and *Nr2f6*$^{-/-}$ mice with a 10-fold higher EG7 tumor load than used in Figure 2. As expected, all wild-type mice rapidly developed tumors and had to be killed latest by day 17 post-injection. In line with our previous results, tumor outgrowth in naive *Nr2f6*$^{-/-}$ mice group was significantly delayed even with this high tumor load. In strict contrast, only one of six memory *Nr2f6*$^{-/-}$ mice had to be killed because of tumor progression at day 41 post-injection; the other five memory *Nr2f6*$^{-/-}$ animals even rejected this higher EG7 cell dose. Accordingly, survival of memory *Nr2f6*$^{-/-}$ mice (80%) was significantly better than the survival of *Nr2f6*$^{+/+}$ mice (0%) or the EG7 antigen-naive *Nr2f6*$^{-/-}$ cohort (20%) (Figures 5C and 5D).

In combination, these results indicate that loss of *Nr2f6* in immune cells strongly enhances tumor immune control. This

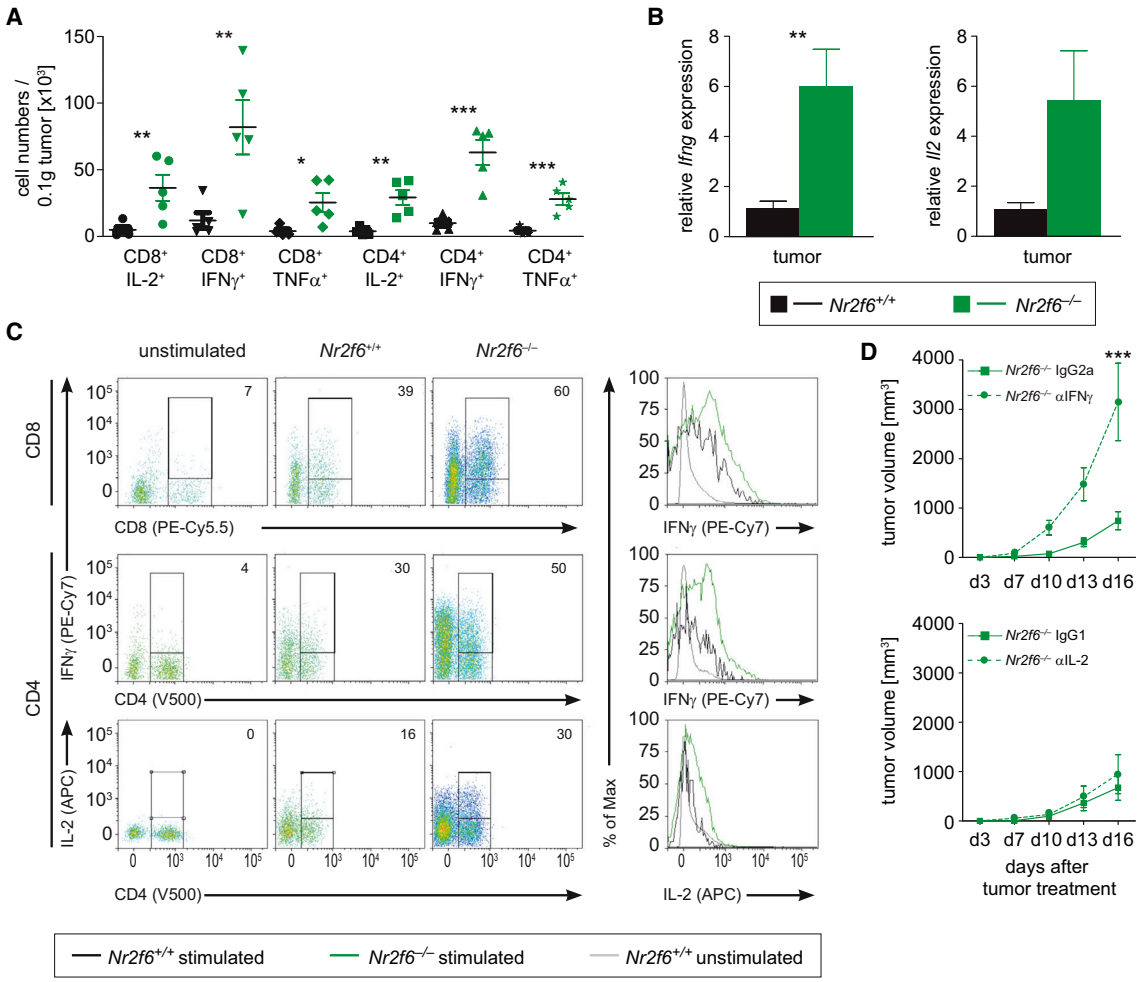

Figure 4. *Nr2f6* Expression Limits Cytokine Secretion of Tumor-Reactive T Cells

(A) Cytokine secretion of *Nr2f6*$^{+/+}$ (n = 6) and *Nr2f6*$^{-/-}$ (n = 7) TILs in tumors larger than 0.022 g revealed significant differences of absolute cell numbers per 0.1 g tumor tissue for the following subsets CD8$^+$IL-2$^+$ (p = 0.01), CD8$^+$IFN-γ$^+$ (p = 0.01), CD8$^+$TNF-α$^+$ (p = 0.002), CD4$^+$IL-2$^+$ (p = 0.002), CD4$^+$IFN-γ$^+$ (p = 0.0006), CD4$^+$TNF-α$^+$ (p = 0.0009) in *Nr2f6*$^{-/-}$ mice.

(B) qRT-PCR analysis of tumors revealed enhanced *Ifng* (p = 0.008) as well as *Il2* expression (p = 0.052) in *Nr2f6*$^{-/-}$ mice. Results shown are derived from at least two independent experiments.

(C) Dot plots and histograms of IFN-γ and IL-2 expressing CD8$^+$ and CD4$^+$ tumor-infiltrating cells gated on CD45$^+$CD3$^+$ T cells derived from *Nr2f6*$^{+/+}$ and *Nr2f6*$^{-/-}$ mice. Numbers indicate percentage of positive gated cells. Results shown are derived from at least two independent experiments. Error bars represent SEM; data were analyzed via Student's t test.

(D) Tumor growth was monitored in *Nr2f6*$^{-/-}$ mice injected s.c. with 5 × 10^5 B16-OVA melanoma cells and administered with 0.5 mg of either an anti-mouse IFN-γ (n = 5) or an anti-mouse IL-2 (n = 3) neutralizing antibody or an corresponding IgG1 or IgG2a control every 3 days starting from day 1 of B16-OVA challenge. Comparison with relevant IgG control revealed disrupted tumor protection in *Nr2f6*$^{-/-}$ mice treated with anti-mouse IFN-γ neutralizing antibody (p = 0.006), but not anti-mouse IL-2 neutralizing antibody (p = 0.4). Summary graphs are the mean ± SEM, statistically analyzed by two-way ANOVA.

striking survival benefit for tumor-bearing *Nr2f6*-deficient mice was accompanied by a host-protective induction of immunological memory, which is well known to depend strongly on the T cell compartment.

T Cell Intrinsic Function of NR2F6 in Cancer Immune Surveillance

To define the role of T cells for tumor rejection in *Nr2f6*$^{-/-}$ mice, we next analyzed EG7 subcutaneous tumor growth in age- and sex-matched *Rag1*$^{-/-}$ mice reconstituted with T cells derived from either *Nr2f6*$^{+/+}$ or *Nr2f6*$^{-/-}$ mice (designated as *Rag1*$^{-/-}$CD3$^{Nr2f6+/+}$ and *Rag1*$^{-/-}$CD3$^{Nr2f6-/-}$, respectively). Similar to the immunocompetent mice, tumor growth was again strongly reduced in *Rag1*$^{-/-}$CD3$^{Nr2f6-/-}$ when compared to *Rag1*$^{-/-}$CD3$^{Nr2f6+/+}$ reconstituted mice (Figures 5E and S5B). Again, T cell numbers in the dLNs were markedly increased (Figures 5F and S5C). Transfer experiments using immunocompetent mice (that also have endogenous immunosuppressive T cells, such as Treg) similarly to the previous experiments demonstrated that adoptive transfer of model tumor

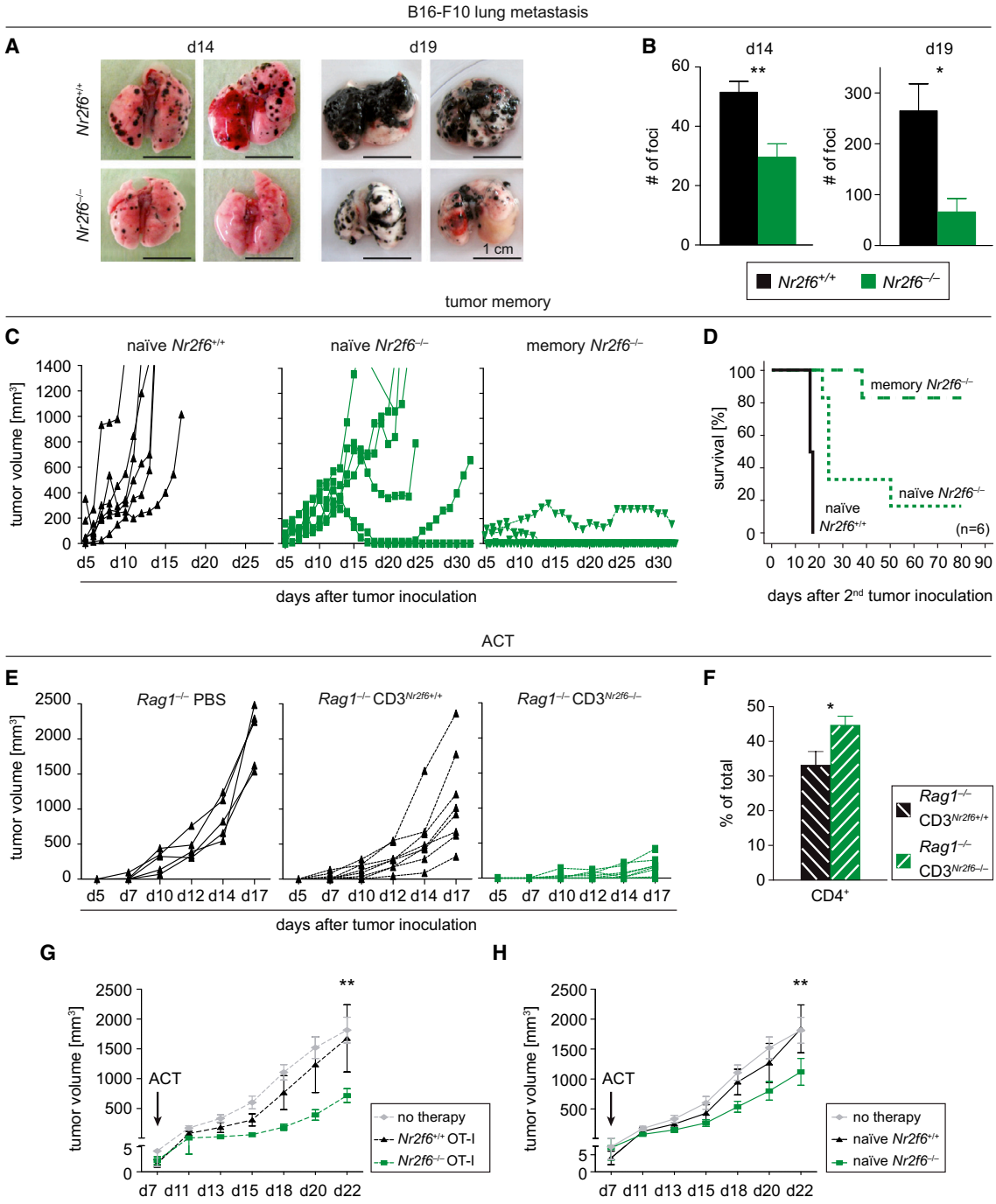

Figure 5. Reduced Metastasis and Anti-Tumor Memory Depends on NR2F6 in T Cells

(A) Gross examination of representative metastatic tumor lungs at day 14 and day 19 after tumor inoculation of either *Nr2f6*$^{+/+}$ mice (n = 10) or *Nr2f6*$^{-/-}$ mice (n = 9) i.v.-injected B16-F10.

(B) Bar chart depict numbers of lung tumor foci on day 14 (p = 0.002) and day 19 (p = 0.02) after tumor induction in *Nr2f6*$^{+/+}$ mice and *Nr2f6*$^{-/-}$ mice.

(C) Long-lasting anti-tumor memory is demonstrated after injection of EG7 tumor cells: *Nr2f6*$^{-/-}$ mice (n = 6), which had received 1.5 × 10^5 EG7 cells subcutaneously at 8–12 weeks of age and rejected the primary tumor, were subsequently re-challenged after 10 months with a 10-fold higher dose of EG7 cells. In contrast to age- and sex-matched naive *Nr2f6*$^{+/+}$ mice (n = 6) and naive *Nr2f6*$^{-/-}$ mice (n = 6) controls, 80% of memory *Nr2f6*$^{-/-}$ mice were able to reject the 10-fold higher tumor dose.

(D) Kaplan-Meier survival curves of age-matched naive *Nr2f6*$^{+/+}$, naive *Nr2f6*$^{-/-}$, and memory *Nr2f6*$^{-/-}$ mice that received 1.5 × 10^6 EG7 cells subcutaneously (p < 0.001), statistically analyzed by log-rank test.

(legend continued on next page)

antigen-specific T cells isolated from OT-I T cell receptor (TCR) transgenic animals crossed to the *Nr2f6*$^{-/-}$ background (Figure 5G) and even polyclonal T cells from *Nr2f6*-deficient animals are sufficient to confer a significant tumor growth delay (Figure 5H). Taken together, these data validate the importance of NR2F6 as T cell-intrinsic suppressor of T cell-mediated tumor growth control in vivo.

NR2F6 Represses Key Cytokine Transcription in Effector CD4$^+$ Th1 and CD8$^+$ T Cells

Next, we investigate the underlying molecular mechanisms mediating enhanced anti-tumor immune reactivity in *Nr2f6*$^{-/-}$ mice and particularly increased cytokine production in *Nr2f6*$^{-/-}$ CD4$^+$ T cells in vitro. Intriguingly, the established repressor of the antigen receptor activation threshold NR2F6 in Th17 cells (Hermann-Kleiter et al., 2008) is substantially upregulated upon in vitro CD3/CD28 stimulation in CD4$^+$ T cells (Figure 6A), indicating a dynamic regulation of *Nr2f6* expression as a potential negative feedback loop limiting CD4$^+$ T cell activation. When culturing wild-type and *Nr2f6*-deficient naive CD4$^+$ T cells under Th1 conditions, cytokine expression pattern analyses confirmed enhanced cytokine responses for IL-2, IFN-γ and TNF-α (Figures 6B–6E). Of note, in contrast to its negative regulatory role for effector T cell biology, NR2F6 is not required for CD4$^+$ Treg cell function (Figures S6A–S6F).

Similar to CD4$^+$ T cells, expression of *Nr2f6* mRNA is low in resting CD8$^+$ T cells, whereas its expression level is strongly induced upon CD3/CD28 stimulation in a time-dependent manner both in murine and human CD8$^+$ T cells (Figures 7A and 7B). Reminiscent to the in vivo data generated in the different tumor models, deficiency of the murine *Nr2f6* gene is associated with significantly elevated IL-2, IFN-γ, and TNF-α secretion levels in CD8$^+$ T cells after CD3/CD28 stimulation, as shown by quantification of secreted cytokines as well as intracellular staining and fluorescence-activated cell sorting (FACS) (Figures 7C and S7A). Accordingly, qRT-PCR revealed significantly enhanced transcript levels of *Il2*, *Ifng*, and *Tnfa* as well as *Il21, Tbx21, Il2ra* mRNA when compared to wild-type T cells (Figure 7D). Enhanced cytokine secretion was not attributable to altered survival of *Nr2f6*$^{-/-}$ CD8$^+$ and CD4$^+$ T cells, respectively (Figures 7E, S6G, S6H, and S7B). Of note, *Nfat2* but not *Nfat1 mRNA* was found to be strongly enhanced in *Nr2f6*-deficient T cells (Figure 7F). NFAT2 protein levels are known to be markedly induced by constitutively expressed NFAT1 upon T cell activation (Serfling et al., 2006). By directly binding to promoters with NFAT, where it is thought to, i.e., actively suppress NFAT/AP-1-mediated gene transcription, NR2F6 simultaneously antagonizes the well-established amplification of *Nfat2* transcription, together maintaining the level of DNA-bound NFAT proteins below what is required for robust transcriptional activation of the *Il2* and *Ifng* promoters.

Mechanistically, we have previously established that NR2F6 is able to directly suppress DNA binding of the activation-dependent transcription factor NFAT at promoter regions within the *Il17* locus in Th17-polarized CD4$^+$ T cells (Hermann-Kleiter et al., 2012). Employing band-shift assays in CD8$^+$ T cells, we complement our recent findings by demonstrating augmented NFAT/AP-1 binding to their bona fide consensus motif defined within the minimal *Il2* promoter region in *Nr2f6*$^{-/-}$ T cells (Figures 7G and S7C). Using chromatin immunoprecipitation (ChIP), we further show that NR2F6 directly binds to the *Il2* promoter in resting wild-type CD8$^+$ T cells; its DNA-binding capability is reduced in a dose-dependent manner upon CD3/CD28 cross-linking (Figures 7H and S7D). Complementary NFAT2 binding at the *Il2* minimal promoter locus, as demonstrated by ChIP analysis, increases in a stimulation-dependent manner that is strongly enhanced in the *Nr2f6*$^{-/-}$ T cells (Figure S7D). Transcription factor binding analysis (Matys et al., 2006) revealed NFAT – NR2F6 DNA binding sites also at the defined distal regulatory region (−1.4 kb) (Ono et al., 2007) as well as at the minimal *Ifng* promoter. Consistently, ChIP analyses with NR2F6 and NFAT2 revealed binding of NR2F6 to these regions in resting cells and enhanced NFAT binding capability in activated *Nr2f6*-deficient T cells (Figures S7E and S7F).

Taken together, the data indicate that T cell-intrinsic NR2F6 directly antagonizes the DNA binding capabilities of the NFAT/AP-1 complex *on the Il2* and *Ifng* promoters, thereby inhibiting the antigen receptor-mediated amplitude of cytokine transcription of these established NFAT/AP-1-dependent target genes. As a consequence, enhanced IL-2 and IFN-γ secretion in *Nr2f6*$^{-/-}$ mice favors T cell-mediated cancer cell elimination, which may, at least in part, explain the improved anti-tumor immunity.

DISCUSSION

Uncovering mechanisms that govern immune control of cancer is of high clinical relevance to further develop improved immune-oncological therapies (Chen and Mellman, 2013; Galon et al., 2013; Motz and Coukos, 2013; Zitvogel et al., 2013). In the present study, we describe that NR2F6 plays a crucial role for effector T cell-dependent anti-tumor immunity. First, we defined the enhanced survival of *Nr2f6*-deficient tumor-bearing

(E) Enhanced tumor rejection is dependent on *Nr2f6*$^{-/-}$ T lymphocytes. The kinetics of tumor cell growth in *Rag1*$^{-/-}$ mice reconstituted with PBS, 1 × 10^7 CD3$^+$ *Nr2f6*$^{+/+}$, or 1 × 10^7 CD3$^+$ *Nr2f6*$^{-/-}$ T cells. The average size of *Rag1*$^{-/-\ PBS}$ tumors at 17 days was 2,034 mm^3 (±156 SEM; n = 5), compared with 1,131 mm^3 (±269 SEM; n = 8) in *Rag1*$^{-/-}$CD3$^{Nr2f6+/+}$ and 138 mm^3 (±54 SEM; n = 8; p < 0.01) in *Rag1*$^{-/-}$CD3$^{Nr2f6-/-}$ mice. One-half of the mice were killed at day 17 after tumor induction in order to analyze tumor dLNs.

(F) Flow cytometry analyses revealed increased CD4$^+$ T cell numbers in the dLNs of tumor-bearing *Rag1*$^{-/-}$CD3$^{Nr2f6-/-}$ mice (p = 0.03) when compared to tumor dLNs of *Rag1*$^{-/-}$CD3$^{Nr2f6+/+}$. The data are depicted as bar chart representing CD4$^+$ cells as percentage of total cells. Summary graphs show the mean ± SEM and were statistically analyzed by Student's t test.

(G and H) Adoptive transfer of *Nr2f6*$^{-/-}$ but not *Nr2f6*$^{+/+}$ CD3$^+$ or OT-I cells into B16-OVA tumor-bearing wild-type mice significantly reduces tumor growth. (G) Kinetics of B16-OVA tumor growth after a single therapeutic adoptive transfer of 3 × 10^6 OT-I donor T cells derived from either *Nr2f6*$^{-/-}$ or *Nr2f6*$^{+/+}$ mice (p = 0.0083) or (H) after single transfer of 1 × 10^7 CD3$^+$ T cells again derived from either *Nr2f6*$^{-/-}$ or *Nr2f6*$^{+/+}$ mice into wild-type mice on day 7 after tumor induction (p = 0.001). Data are representative of at least two independent experiments (naive recipients n ≥ 7/group, OT-I recipients n = 6/group); graphs show the mean ± SEM statistically analyzed by two-way ANOVA.

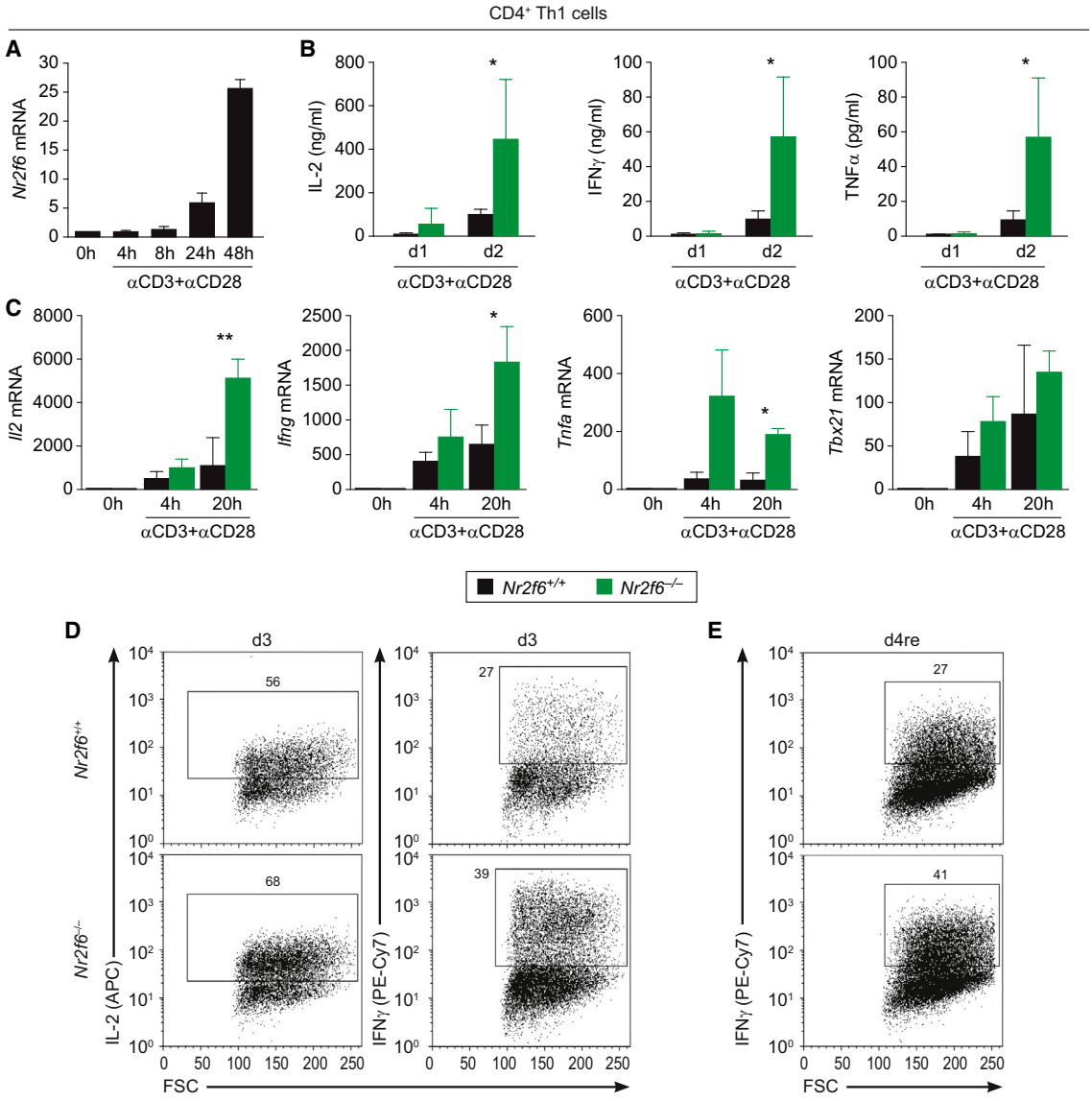

Figure 6. *Nr2f6* Suppresses Th1 CD4⁺ T Cell Activation

(A) In vitro qRT-PCR analysis of *Nr2f6* mRNA in wild-type CD4⁺ T cells during Th1 differentiation activated with anti-CD3 mAb (5 μg) and anti-CD28 mAb (1 μg) at the indicated time points (n = 3).

(B) Bioplex technology was used to demonstrate significantly increased secretion of the pro-inflammatory cytokines IL-2 (p = 0.045), IFN-γ (p = 0.047), and TNF-α (p = 0.046) in the supernatant of in-vitro-activated *Nr2f6*$^{-/-}$ versus wild-type CD4⁺ T cells at day 1 and day 2 of differentiation under Th1-polarizing conditions (n = 3).

(C) In vitro qRT-PCR analysis similarly detected enhanced transcript expression levels of *Il2* (p = 0.003), *Ifng* (p = 0.044), *Tnfa* (p = 0.017), but not *Tbx21* (p = 0.17) mRNA in *Nr2f6*$^{-/-}$ CD4⁺ Th1 cells compared to *Nr2f6*$^{+/+}$ cells upon activation with anti-CD3 (5 μg) and anti-CD28 (1 μg) at the indicated time points (n = 3). Expression was normalized to the housekeeping gene GAPDH and presented as fold induction of unstimulated cells. Summary graphs represent the mean ± SD, data are representative for at least two independent experiments, and statistical differences were evaluated by applying two-way ANOVA.

(D and E) (D) Analysis of IL-2 and IFN-γ producing CD4⁺ Th1 T *Nr2f6*$^{+/+}$ or *Nr2f6*$^{-/-}$ cells by flow cytometry after 3 days (3d) of Th1 driving conditions and (E) followed by a restimulation with anti-CD3 (5 μg) overnight (d4/re). Numbers within outlined areas indicate the percentage of cytokine-expressing cells, and one out of three representative experiments is shown.

mice and their superior immune cell composition using the prostate tumor model TRAMP. Second, we validated these findings by using various transplantable tumor models showing the survival benefit and the induction of a protective anti-tumor immune response including long-lasting immunological memory in *Nr2f6*-deficient mice. Third, we highlight that the observed anti-tumor effects depend on NR2F6 function in T cells, as adoptive transfer of both OT-I TCR-transgenic and even polyclonal *Nr2f6*-deficient T cells into tumor-bearing immunocompetent wild-type mice is sufficient to delay tumor growth.

Albeit one cannot exclude the possibility that other immune or non-immune cells are at least to some extent involved, consistent results generated in all of our experimental approaches validate the negative regulatory role of NR2F6 during T cell activation in cancer. Thus, NR2F6 acts as a bona fide intracellular immune checkpoint in T cells. This statement is further supported by our finding that NR2F6 deletion is equally effective than blocking PD-1/PD-L1 interaction as an established immune-checkpoint mechanism.

We observed significantly elevated numbers of tumor-infiltrating $CD4^+$ and $CD8^+$ T cells, as well as increased IL-2, IFN-γ, and TNF-α secretion rates in ex vivo analysis as well as at the tumor site in *Nr2f6*$^{-/-}$ tumor-bearing mice. Deficiency of *Nr2f6* thus leads to T cells with an a priori lowered TCR activation threshold, finally resulting in enhanced cytokine secretion of IL-2 as an established key cytokine potently favoring tumor rejection (reviewed by Liao et al., 2013). Along this line, we also observed increased production of IFN-γ by effector T cells. Importantly, IFN-γ has been shown to play a pivotal role in tumor-protective immune responses (Weiss et al., 2011): it is critically required for the "productive" immune surveillance of spontaneous malignancies and chemical carcinogen methylcholanthrene (MCA)-induced sarcomas, immune memory formation, and especially senescence of cancer cells (Braumüller et al., 2013).

Mechanistically, our data suggest that NR2F6 acts as a transcriptional suppressor of NFAT/AP-1-mediated signaling in T cells and its deletion results in enhanced sensitivity to CD3/CD28 activation. Similar to the action of other NRs, NR2F6 appears to directly bind to sites that are otherwise occupied by NFAT/AP-1 to prevent transcriptional activation. This supports a model in which the balance of pre-bound NR2F6 versus TCR-triggered NFAT/AP-1 DNA-binding-capabilities directly dictates the outcome of, e.g., IFN-γ cytokine production. As NFAT/AP-1 transcription factors are known to bind to the *Il2*, *Ifng*, *and Tnfa* promoters, it is therefore likely that NR2F6 mediates its suppressive effects in tumor-reactive effector $CD4^+$ Th1 and $CD8^+$ T cells via this cell-intrinsic mechanism. Importantly, however, CD3/CD28-induced activation apparently leads to an induced displacement of NR2F6 from the given cytokine promoter, thereby promoting unopposed DNA binding of NFAT/AP-1-complexes at the critical cytokine gene loci.

The immunological microenvironment observed in *Nr2f6*-deficient tumor-bearing mice assemble a positive immune contexture potentially supporting cancer cell rejection. This hypothesis is strengthened by correlative clinical data showing that an increased rate of tumor-infiltrating T cells is an important predictor of clinical outcome in cancer patients (reviewed in Galon et al., 2013; Fridman et al., 2012). Moreover, increased expression levels of PD-1 within the TIL compartment in *Nr2f6*$^{-/-}$ mice fit to the recent observation that PD-1-expressing $CD8^+$ T cells are the tumor-reactive ones (Gros et al., 2014). Intriguingly, *Nr2f6* is substantially upregulated ex vivo in CD3/CD28-stimulated $CD4^+$ and $CD8^+$ T cell cultures, respectively, indicating a dynamic regulation of *Nr2f6* expression as a negative feedback loop. *Nr2f6* gene ablation therefore results in immune response outcomes that, albeit by a different mode of action, appears reminiscent to the blockade of immune tolerance signaling induced by CTLA-4 or PD-1/PD-L1 (Robert et al., 2011; Hodi et al., 2010; Hamid et al., 2013; Brahmer et al., 2010; Chen and Mellman, 2013; Fridman et al., 2012; Powles et al., 2014; Tumeh et al., 2014).

Interestingly, a correlation of NR2F6 expression and human cancer has been observed: a compendium of data sets indicates that *Nr2f6* expression is predominately upregulated in human ovarian cancer, colon cancer, and lymphoma (King et al., 2011; Li et al., 2011; Eckerle et al., 2009; Ichim et al., 2011). Genome-wide association studies and expression analysis have linked NR2F6 to breast cancer, when compared with the expression pattern of the other 46 human nuclear receptors (Antoniou et al., 2010; Muscat et al., 2013). Although it is impossible from these published data sets to determine whether the origin of NR2F6 expression is the malignant or the immune cell, in one breast cancer study tumor-infiltrating T cells were isolated and shown to have upregulated *Nr2f6* expression compared to peripheral T cells (Gu-Trantien et al., 2013).

Because of the established T cell dysfunction as a consequence of cancer-mediated immunosuppression, our data strongly suggest that T cell-based therapies could significantly benefit from modulation of this NR2F6 inhibitory signaling pathway. Importantly, the ligand binding domain (LBD) on NR2F6 is evolutionarily highly conserved and appears to be essential for NR2F6 transcriptional repressor activity (Hermann-Kleiter et al., 2012). This potential drugability of its LBD for a "small molecule checkpoint blockade drug" may provide a rational mechanistic basis envisioning targeted manipulation of NR2F6 in T cells as a promising intracellular checkpoint-targeting strategy to improve the efficacy and broaden the applicability of cancer immunotherapy regimens, finally enabling prolonged patient survival.

In sum, orphan nuclear receptor NR2F6 appears to be an intracellular immune checkpoint, directly repressing transcription of cytokine genes in T cells relevant for cancer cell rejection, such as IL-2, IFN-γ, and TNF-α. Thus, in the presence of NR2F6 effector T cell activation is limited within the tumor microenvironment. The exact molecular pathway by which NR2F6 impairs the transcriptional amplitude of NFAT/AP-1 gene transactivation including all target genes of NR2F6 demands further investigations.

EXPERIMENTAL PROCEDURES

Mice

Nr2f6-deficient mice (Warnecke et al., 2005) backcrossed on C57BL/6 background were used. Wild-type C57BL/6 TRAMP (Tg[TRAMP]8247Ng) mice were crossed into *Nr2f6*-deficient mice to generate *Nr2f6*$^{-/-\text{TRAMP}}$ and *Nr2f6*$^{+/+\text{TRAMP}}$ mice. All animal experiments have been performed in accordance with national and European guidelines and have been reviewed and authorized by the committee on animal experiments (BMWFW-66.0ll/0128-WF/V/3b/2014).

Tumor Induction and Adoptive Cell Transfer

1×10^5 B16-OVA, 3×10^5 B16-F10 cells, 1.5×10^5 EG7 cells, or 1×10^6 TRAMP-C1 cells (purchased from the ATCC, CRL-2730) were injected subcutaneously (s.c.) into the left flank of 8- to 12-week-old mice. Tumor memory experiments were performed via s.c. injection of 1.5×10^6 EG7 cells into 1-year-old *Nr2f6*$^{-/-}$ mice, which rejected primary tumor challenge. Tumor growth was monitored three times per week by measuring tumor length and width. Tumor volume was calculated according to the following equation: 1/2(length × width^2). For survival analysis, mice with tumors greater than the length limit of 15 mm were sacrificed and counted as dead.

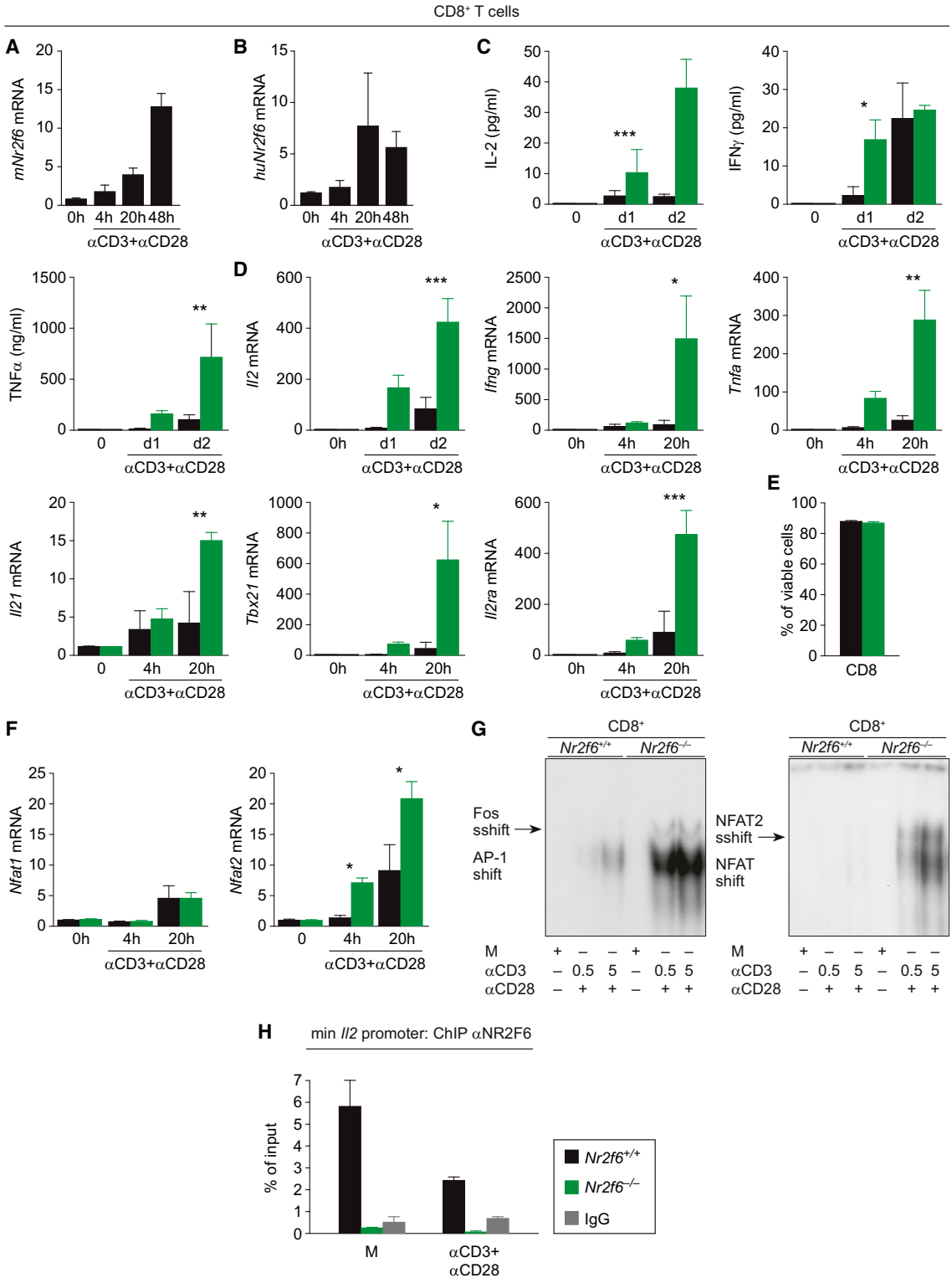

Figure 7. *Nr2f6* Suppresses CD8⁺ T Cell Activation

(A and B) *Nr2f6* expression is induced in a TCR-dependent manner in both (A) mice and (B) human CD8⁺ T cells activated with anti-CD3 (5 μg) and anti-CD28 (1 μg) in vitro (n = 3).

(legend continued on next page)

Preparation of Tumor-Infiltrating Cells

Mononuclear infiltrating cells were isolated from both subcutaneous and autochthonous tumors at the indicated time points. Briefly, tumor tissues from sacrificed mice were prepared by mechanical disruption followed by digestion for 45 min with collagenase D (2.5 mg/ml; Roche, 11088858001) and DNase I (1 mg/ml; Roche, 11284932001) at 37°C. Digested tissues were incubated 5 min at 37°C with EDTA (0.5 M) to prevent DC/T cell aggregates and mashed through filters.

Statistics

Data were analyzed using Prism 5.03 software (GraphPad). Experiments were repeated at least two or three times. Data are represented as indicated (either mean ± SEM or ± SD) for all figure panels in which error bars are shown. The p values were assessed using two-tailed unpaired Student's t test, log-rank test, or ANOVA. A p value of <0.05 was considered statistically significant: $^{*}p < 0.05$; $^{**}p < 0.01$; $^{***}p < 0.001$.

SUPPLEMENTAL INFORMATION

Supplemental Information includes Supplemental Experimental Procedures and seven figures and can be found with this article online at http://dx.doi.org/10.1016/j.celrep.2015.08.035.

AUTHOR CONTRIBUTIONS

All authors have contributed substantially to the work. S.W., K.S., S. Klepsch, S.T., S. Kaminski, A.V., T.G., and C.P.-O. performed key experiments and/or analyses of the data. N.H.-K. outlined and performed the overall experimental design of tumor and memory experiments, in vitro experiments, ChIP analysis, and qRT-PCR, prepared figures, and wrote the initial paper draft; V.K. performed flow cytometry, tumor, and adoptive transfer experiments. G.B. and D.W. provided the study conception, and G.B. provided the overall supervision of the research at all stages.

ACKNOWLEDGMENTS

This work was supported by grants from the FFG Austrian Research Promotion Agency (BRIDGE-842388-CBL-AIM) and FWF Austrian Science Fund (W1101-B18, P23537-B13, P25044-B21, "Hertha-Firnberg" T264-B13, and "Lise-Meitner" M1636-B23), the Austrian Cancer Society, Tyrol as well as the Deutsche Forschungsgemeinschaft (DFG WO1877/1-1). We are grateful to Michaela Kind and Nina Posch (both from our institute in Innsbruck) for technical assistance.

Received: May 9, 2014
Revised: July 2, 2015
Accepted: August 11, 2015
Published: September 17, 2015

REFERENCES

Antoniou, A.C., Wang, X., Fredericksen, Z.S., McGuffog, L., Tarrell, R., Sinilnikova, O.M., Healey, S., Morrison, J., Kartsonaki, C., Lesnick, T., et al.; EMBRACE; GEMO Study Collaborators; HEBON; kConFab; SWE-BRCA; MOD SQUAD; GENICA (2010). A locus on 19p13 modifies risk of breast cancer in BRCA1 mutation carriers and is associated with hormone receptor-negative breast cancer in the general population. Nat. Genet. *42*, 885–892.

Bedognetti, D., Spivey, T.L., Zhao, Y., Uccellini, L., Tomei, S., Dudley, M.E., Ascierto, M.L., De Giorgi, V., Liu, Q., Delogu, L.G., et al. (2013). CXCR3/CCR5 pathways in metastatic melanoma patients treated with adoptive therapy and IL-2. Br. J. Cancer *109*, 2412–2423.

Bodor, J., Bopp, T., Vaeth, M., Klein, M., Serfling, E., Hünig, T., Becker, C., Schild, H., and Schmitt, E. (2012). Cyclic AMP underpins suppression by regulatory T cells. Eur. J. Immunol. *42*, 1375–1384.

Brahmer, J.R., Drake, C.G., Wollner, I., Powderly, J.D., Picus, J., Sharfman, W.H., Stankevich, E., Pons, A., Salay, T.M., McMiller, T.L., et al. (2010). Phase I study of single-agent anti-programmed death-1 (MDX-1106) in refractory solid tumors: safety, clinical activity, pharmacodynamics, and immunologic correlates. J. Clin. Oncol. *28*, 3167–3175.

Braumüller, H., Wieder, T., Brenner, E., Aßmann, S., Hahn, M., Alkhaled, M., Schilbach, K., Essmann, F., Kneilling, M., Griessinger, C., et al. (2013). T-helper-1-cell cytokines drive cancer into senescence. Nature *494*, 361–365.

Chen, D.S., and Mellman, I. (2013). Oncology meets immunology: the cancer-immunity cycle. Immunity *39*, 1–10.

Eckerle, S., Brune, V., Döring, C., Tiacci, E., Bohle, V., Sundström, C., Kodet, R., Paulli, M., Falini, B., Klapper, W., et al. (2009). Gene expression profiling of isolated tumour cells from anaplastic large cell lymphomas: insights into its cellular origin, pathogenesis and relation to Hodgkin lymphoma. Leukemia *23*, 2129–2138.

Fridman, W.H., Pagès, F., Sautès-Fridman, C., and Galon, J. (2012). The immune contexture in human tumours: impact on clinical outcome. Nat. Rev. Cancer *12*, 298–306.

Galon, J., Angell, H.K., Bedognetti, D., and Marincola, F.M. (2013). The continuum of cancer immunosurveillance: prognostic, predictive, and mechanistic signatures. Immunity *39*, 11–26.

Greenberg, N.M., DeMayo, F., Finegold, M.J., Medina, D., Tilley, W.D., Aspinall, J.O., Cunha, G.R., Donjacour, A.A., Matusik, R.J., and Rosen, J.M. (1995). Prostate cancer in a transgenic mouse. Proc. Natl. Acad. Sci. USA *92*, 3439–3443.

Gros, A., Robbins, P.F., Yao, X., Li, Y.F., Turcotte, S., Tran, E., Wunderlich, J.R., Mixon, A., Farid, S., Dudley, M.E., et al. (2014). PD-1 identifies the patient-specific $CD8^{+}$ tumor-reactive repertoire infiltrating human tumors. J. Clin. Invest. *124*, 2246–2259.

Gu-Trantien, C., Loi, S., Garaud, S., Equeter, C., Libin, M., de Wind, A., Ravoet, M., Le Buanec, H., Sibille, C., Manfouo-Foutsop, G., et al. (2013). $CD4^{+}$ follicular

(C) Bioplex technology was used to analyze the secretion of IL-2 ($p = 0.0002$), IFN-γ ($p = 0.03$), and TNF-α ($p = 0.016$) in the supernatant of in vitro activated murine $CD8^{+}$ T cells at day 1 and day 2 ($n = 3$).

(D) qRT-PCR analysis of in-vitro-stimulated *Nr2f6*$^{+/+}$ and *Nr2f6*$^{-/-}$ $CD8^{+}$ T cells at the indicated time points revealed enhanced *Il2* ($p = 0.0003$), *Ifng* ($p = 0.02$), *Tnfa* ($p = 0.002$), *Il21* ($p = 0.002$), *Tbx21* ($p = 0.02$), and *Il2ra* ($p = 0.0006$) expression levels ($n = 3$). Expression was normalized to the housekeeping gene GAPDH and presented as fold induction versus unstimulated controls. Summary graphs represent the mean ± SD, data are representative of at least two independent experiments, and statistics were calculated using two-way ANOVA.

(E) Using FACS, $CD4^{+}$ T cells were sorted from *Nr2f6*$^{+/+}$ and *Nr2f6*$^{-/-}$ mice and stimulated in vitro with plate-bound anti-CD3 (5 μg/ml) plus soluble anti-CD28 (1 μg/ml). Viability was assessed by Annexin V/Propidiumiodid (PI) staining in a flow cytometer after 48 hr.

(F) qRT-PCR analysis of in-vitro-stimulated *Nr2f6*$^{+/+}$ and *Nr2f6*$^{-/-}$ $CD8^{+}$ T cells revealed enhanced *Nfat2* ($p = 0.015$) expression levels ($n = 3$).

(G) *Nr2f6*$^{+/+}$ and *Nr2f6*$^{-/-}$ $CD8^{+}$ T cells were activated with anti-CD3 (0.5 or 5 μg) and anti-CD28 (1 μg) for 20 hr in vitro, nuclear extracts were isolated, and electromobility assays were performed for AP-1 and NFAT2. AP-1 and NFAT2 DNA binding is induced in an anti-CD3 mAb concentration-dependent manner and was strongly enhanced in *Nr2f6*$^{-/-}$ $CD8^{+}$ T cells. Supershift analysis was performed by using antibodies against c-*fos* and NFAT2 as indicated. Loading was controlled by immunoblotting of lamin B using the corresponding nuclear extracts (Figure S7C). One representative experiment out of three is shown.

(H) Nr2f6 binding to the *Il2* promoter was evaluated by ChIP. Therefore, either *Nr2f6*$^{+/+}$ or *Nr2f6*$^{-/-}$ $CD8^{+}$ resting or activated for 20 hr with anti-CD3 (5 μg) and anti-CD28 (1 μg) activated cells were used with anti-NR2F6 or IgG control, and *cytokine* promoter sequence was quantified by real-time PCR. The data are presented as percentage of input samples before immunoprecipitation.

helper T cell infiltration predicts breast cancer survival. J. Clin. Invest. *123*, 2873–2892.

Gubin, M.M., Zhang, X., Schuster, H., Caron, E., Ward, J.P., Noguchi, T., Ivanova, Y., Hundal, J., Arthur, C.D., Krebber, W.J., et al. (2014). Checkpoint blockade cancer immunotherapy targets tumour-specific mutant antigens. Nature *515*, 577–581.

Hamid, O., Robert, C., Daud, A., Hodi, F.S., Hwu, W.J., Kefford, R., Wolchok, J.D., Hersey, P., Joseph, R.W., Weber, J.S., et al. (2013). Safety and tumor responses with lambrolizumab (anti-PD-1) in melanoma. N. Engl. J. Med. *369*, 134–144.

Hermann-Kleiter, N., Gruber, T., Lutz-Nicoladoni, C., Thuille, N., Fresser, F., Labi, V., Schiefermeier, N., Warnecke, M., Huber, L., Villunger, A., et al. (2008). The nuclear orphan receptor NR2F6 suppresses lymphocyte activation and T helper 17-dependent autoimmunity. Immunity *29*, 205–216.

Hermann-Kleiter, N., Meisel, M., Fresser, F., Thuille, N., Müller, M., Roth, L., Katopodis, A., and Baier, G. (2012). Nuclear orphan receptor NR2F6 directly antagonizes NFAT and RORγt binding to the *Il17a* promoter. J. Autoimmun. *39*, 428–440.

Hodi, F.S., O'Day, S.J., McDermott, D.F., Weber, R.W., Sosman, J.A., Haanen, J.B., Gonzalez, R., Robert, C., Schadendorf, D., Hassel, J.C., et al. (2010). Improved survival with ipilimumab in patients with metastatic melanoma. N. Engl. J. Med. *363*, 711–723.

Hunder, N.N., Wallen, H., Cao, J., Hendricks, D.W., Reilly, J.Z., Rodmyre, R., Jungbluth, A., Gnjatic, S., Thompson, J.A., and Yee, C. (2008). Treatment of metastatic melanoma with autologous $CD4^+$ T cells against NY-ESO-1. N. Engl. J. Med. *358*, 2698–2703.

Ichim, C.V., Atkins, H.L., Iscove, N.N., and Wells, R.A. (2011). Identification of a role for the nuclear receptor EAR-2 in the maintenance of clonogenic status within the leukemia cell hierarchy. Leukemia *25*, 1687–1696.

Kalos, M., and June, C.H. (2013). Adoptive T cell transfer for cancer immunotherapy in the era of synthetic biology. Immunity *39*, 49–60.

Kantoff, P.W., Schuetz, T.J., Blumenstein, B.A., Glode, L.M., Bilhartz, D.L., Wyand, M., Manson, K., Panicali, D.L., Laus, R., Schlom, J., et al. (2010). Overall survival analysis of a phase II randomized controlled trial of a Poxviral-based PSA-targeted immunotherapy in metastatic castration-resistant prostate cancer. J. Clin. Oncol. *28*, 1099–1105.

King, E.R., Tung, C.S., Tsang, Y.T.M., Zu, Z., Lok, G.T.M., Deavers, M.T., Malpica, A., Wolf, J.K., Lu, K.H., Birrer, M.J., et al. (2011). The anterior gradient homolog 3 (*AGR3*) gene is associated with differentiation and survival in ovarian cancer. Am. J. Surg. Pathol. *35*, 904–912.

Li, X.-B., Jiao, S., Sun, H., Xue, J., Zhao, W.-T., Fan, L., Wu, G.-H., and Fang, J. (2011). The orphan nuclear receptor EAR2 is overexpressed in colorectal cancer and it regulates survivability of colon cancer cells. Cancer Lett. *309*, 137–144.

Liao, W., Lin, J.-X., and Leonard, W.J. (2013). Interleukin-2 at the crossroads of effector responses, tolerance, and immunotherapy. Immunity *38*, 13–25.

Matys, V., Kel-Margoulis, O.V., Fricke, E., Liebich, I., Land, S., Barre-Dirrie, A., Reuter, I., Chekmenev, D., Krull, M., Hornischer, K., et al. (2006). TRANSFAC and its module TRANSCompel: transcriptional gene regulation in eukaryotes. Nucleic Acids Res. *34*, D108–D110.

Motz, G.T., and Coukos, G. (2013). Deciphering and reversing tumor immune suppression. Immunity *39*, 61–73.

Muscat, G.E.O., Eriksson, N.A., Byth, K., Loi, S., Graham, D., Jindal, S., Davis, M.J., Clyne, C., Funder, J.W., Simpson, E.R., et al. (2013). Research resource: nuclear receptors as transcriptome: discriminant and prognostic value in breast cancer. Mol. Endocrinol. *27*, 350–365.

Ono, M., Yaguchi, H., Ohkura, N., Kitabayashi, I., Nagamura, Y., Nomura, T., Miyachi, Y., Tsukada, T., and Sakaguchi, S. (2007). Foxp3 controls regulatory T-cell function by interacting with AML1/Runx1. Nature *446*, 685–689.

Pipkin, M.E., Sacks, J.A., Cruz-Guilloty, F., Lichtenheld, M.G., Bevan, M.J., and Rao, A. (2010). Interleukin-2 and inflammation induce distinct transcriptional programs that promote the differentiation of effector cytolytic T cells. Immunity *32*, 79–90.

Powles, T., Eder, J.P., Fine, G.D., Braiteh, F.S., Loriot, Y., Cruz, C., Bellmunt, J., Burris, H.A., Petrylak, D.P., Teng, S.L., et al. (2014). MPDL3280A (anti-PD-L1) treatment leads to clinical activity in metastatic bladder cancer. Nature *515*, 558–562.

Restifo, N.P., Dudley, M.E., and Rosenberg, S.A. (2012). Adoptive immunotherapy for cancer: harnessing the T cell response. Nat. Rev. Immunol. *12*, 269–281.

Robert, C., Thomas, L., Bondarenko, I., O'Day, S., Weber, J., Garbe, C., Lebbe, C., Baurain, J.F., Testori, A., Grob, J.J., et al. (2011). Ipilimumab plus dacarbazine for previously untreated metastatic melanoma. N. Engl. J. Med. *364*, 2517–2526.

Schwartzentruber, D.J., Lawson, D.H., Richards, J.M., Conry, R.M., Miller, D.M., Treisman, J., Gailani, F., Riley, L., Conlon, K., Pockaj, B., et al. (2011). gp100 peptide vaccine and interleukin-2 in patients with advanced melanoma. N. Engl. J. Med. *364*, 2119–2127.

Serfling, E., Chuvpilo, S., Liu, J., Höfer, T., and Palmetshofer, A. (2006). NFATc1 autoregulation: a crucial step for cell-fate determination. Trends Immunol. *27*, 461–469.

Shankaran, V., Ikeda, H., Bruce, A.T., White, J.M., Swanson, P.E., Old, L.J., and Schreiber, R.D. (2001). IFNgamma and lymphocytes prevent primary tumour development and shape tumour immunogenicity. Nature *410*, 1107–1111.

Topalian, S.L., Drake, C.G., and Pardoll, D.M. (2012). Targeting the PD-1/B7-H1(PD-L1) pathway to activate anti-tumor immunity. Curr. Opin. Immunol. *24*, 207–212.

Tumeh, P.C., Harview, C.L., Yearley, J.H., Shintaku, I.P., Taylor, E.J., Robert, L., Chmielowski, B., Spasic, M., Henry, G., Ciobanu, V., et al. (2014). PD-1 blockade induces responses by inhibiting adaptive immune resistance. Nature *515*, 568–571.

van den Eertwegh, A.J., Versluis, J., van den Berg, H.P., Santegoets, S.J., van Moorselaar, R.J., van der Sluis, T.M., Gall, H.E., Harding, T.C., Jooss, K., Lowy, I., et al. (2012). Combined immunotherapy with granulocyte-macrophage colony-stimulating factor-transduced allogeneic prostate cancer cells and ipilimumab in patients with metastatic castration-resistant prostate cancer: a phase 1 dose-escalation trial. Lancet Oncol. *13*, 509–517.

Warnecke, M., Oster, H., Revelli, J.P., Alvarez-Bolado, G., and Eichele, G. (2005). Abnormal development of the locus coeruleus in *Ear2(Nr2f6)*-deficient mice impairs the functionality of the forebrain clock and affects nociception. Genes Dev. *19*, 614–625.

Weiss, G.R., Grosh, W.W., Chianese-Bullock, K.A., Zhao, Y., Liu, H., Slingluff, C.L., Jr., Marincola, F.M., and Wang, E. (2011). Molecular insights on the peripheral and intratumoral effects of systemic high-dose rIL-2 (aldesleukin) administration for the treatment of metastatic melanoma. Clin. Cancer Res. *17*, 7440–7450.

Zitvogel, L., Tesniere, A., and Kroemer, G. (2006). Cancer despite immunosurveillance: immunoselection and immunosubversion. Nat. Rev. Immunol. *6*, 715–727.

Zitvogel, L., Galluzzi, L., Smyth, M.J., and Kroemer, G. (2013). Mechanism of action of conventional and targeted anticancer therapies: reinstating immunosurveillance. Immunity *39*, 74–88.

Zou, W. (2005). Immunosuppressive networks in the tumour environment and their therapeutic relevance. Nat. Rev. Cancer *5*, 263–274.

Cell Reports

Supplemental Information

The Nuclear Orphan Receptor NR2F6 Is a Central Checkpoint for Cancer Immune Surveillance

Natascha Hermann-Kleiter, Victoria Klepsch, Stephanie Wallner, Kerstin Siegmund, Sebastian Klepsch, Selma Tuzlak, Andreas Villunger, Sandra Kaminski, Christa Pfeifhofer-Obermair, Thomas Gruber, Dominik Wolf, and Gottfried Baier

Supplemental Experimental Procedures

Mice. *Nr2f6*-deficient mice (Warnecke et al., 2005) back-crossed on C57BL/6 background were used. Wild-type C57BL/6 TRAMP (Tg(TRAMP)8247Ng) mice were crossed into *Nr2f6*-deficient mice to generate *Nr2f6*$^{-/-\text{TRAMP}}$ and *Nr2f6*$^{+/+\text{TRAMP}}$ mice. *Rag*1$^{-/-}$ (B6.129S7-*Rag*1$^{\text{tm1Mom}}$/J) mice were provided by A. Moschen and used for adoptive CD3^{+} cell transfer experiments. Mice were maintained under SPF conditions. All animal experiments have been performed in accordance with national and European guidelines and have been reviewed and authorized by the committee on animal experiments (BMWFW-66.0ll/0128-WF/V/3b/2014) .

Tumor induction and adoptive cell transfer. 1×10^{5} B16-OVA, 3×10^{5} B16-F10 cells, 1.5×10^{5} EG7 cells, or 1×10^{6} TRAMP-C1 cells (purchased from the ATCC, CRL-2730) were injected subcutaneously (s.c.) into the left flank of 8- to 12-week-old mice. Tumor memory experiments were performed via s.c. injection of 1.5×10^{6} EG7 cells into 1 year old *Nr2f6*$^{-/-}$ mice, which rejected primary tumor challenge. Tumor growth was monitored three times per week by measuring tumor length and width. Tumor volume was calculated according to the following equation: ½(length × width^{2}). For survival analysis, mice with tumors greater than the length limit of 15 mm were sacrificed and counted as dead. Adoptive cell transfer (ACT) of *Nr2f6*$^{+/+}$ or *Nr2f6*$^{-/-}$ CD3^{+} T cells into *Rag*1$^{-/-}$ mice was performed 14 days prior tumor induction by injecting 1×10^{7} CD3^{+} T using the Pan T Cell Isolation Kit II mouse (Miltenyi Biotech 130-095-130) via intra-peritoneal injection.

***In vivo* antibody blockade**. Mice were injected s.c. with 5x10^{5} B16-OVA melanoma cells and administered with either 0.5mg of an anti-mouse IFNγ (Clone R4-6A2; BE0054; BioXCell), anti-mouse IL-2 (Clone S4B6-1; BE0043-1), anti-mouse PD-L1 (Clone10F.9G2; BE0101) or corresponding IgG1 (Clone 2A3; BE0089), IgG2b (LTF-2; BE0090) or IgG2a (Clone HRPN; BE0088) control (all from BioXCell, USA) every 3 days starting from day 1 of B16-OVA challenge according to (Zou et al., 2014).

Therapeutic adoptive cell transfer. C57BL/6 wild-type mice at 8 to 12 weeks of age were injected with 1×10^{5} B16-OVA melanoma cells and left untreated until day 7 to establish clearly visible tumors. For adoptive transfers CD3^{+} T cells either from *Nr2f6*$^{+/+}$ or *Nr2f6*$^{-/-}$ tumor antigen naïve mice or *Nr2f6*$^{+/+}$ or *Nr2f6*$^{-/-}$ OT-I transgenic mice were isolated using the

Pan T cell Isolation Kit II (Miltenyi Biotec, 130-095-130) and 1×10^7 $CD3^+$ or 3×10^6 OT-I donor T cells were injected intraperitoneally on day 7 after tumor induction and tumor growth was subsequently measured as described above.

Preparation of tumor infiltrating cells. Mononuclear infiltrating cells were isolated from both subcutaneous and autochthonous tumors at the indicated time points. Briefly, tumor tissues from sacrificed mice were prepared by mechanical disruption followed by digestion for 45 min with collagenase D (2.5 mg/ml; Roche, 11088858001) and DNase I (1 mg/ml; Roche, 11284932001) at 37°C. Digested tissues were incubated 5 min at 37°C with EDTA (0.5 M) to prevent DC/T cell aggregates and mashed through a 100-µm filter and a 40-µm filter. Cells were washed, and resuspended in either PBS+2% FCS or IMDM complete medium (10% FCS, 2 mM L-glutamine, and 50 U/ml penicillin/streptomycin).

***Ex vivo* $CD8^+$ T cell analysis**. $CD8^+$ T cells were isolated using either the mouse CD8 T Cell Isolation Kit II (Miltenyi Biotec, 130-090-859) or the human $CD8^+$ T Cell Isolation Kit (Miltenyi Biotec, 130-096-495). Activation of $CD8^+$ T cells was performed in complete IMDM medium in the presence of plate-bound 2C11 (made in house) for mouse or OKT3 for human anti-CD3 (5 µg/ml, eBiosciences, 16-0037) and soluble mouse or human anti-CD28 (1 µg/ml, BD, 553294). Cells were harvested at the indicated time points. For survival and apoptosis assays, spleens and lymph nodes were isolated from *Nr2f6*$^{+/+}$ and *Nr2f6*$^{-/-}$ mice. Single cell suspensions were pooled and stained with fluorochrome-labelled antibodies recognizing mouse CD4 (GK1.5) or mouse CD8a (53-6.7, both from BioLegend), respectively. To exclude dead cells, 12.5µg/mL DAPI was added. Cells were sorted on a BD FacsAria^{TM}III Cell sorter (BD Biosciences). Sorted T cells were cultured at a concentration of $1x10^6$/mL in Roswell Park Memorial Institute (RPMI) 1640 medium (PAA; E15-039), supplemented with 10% FCS, 2 mM L-Glutamine, 1% Penicillin plus Streptomycin (10.000 U/mL Penicillin and 10 mg/mL Streptomycin in 0.9% NaCl), 5×10^{-5} M 2-mercaptoethanol, 50µg/mL Gentamicin, 100µM non-essential amino acids (Gibco, 1091607) and 1 mM sodium pyruvate (Gibco, 1046485). Apoptosis was assessed after 48 hours in culture using Annexin V Apoptosis Detection Kit eFluor® 450 (eBioscience).

Chromatin immunoprecipitation. ChIP assay was performed with a ChIP assay kit according to the recommendations of the manufacturer (Imgenex) in combination with the Cold Spring Harbor protocol (Carey et al., 2009) and previously described methods (Hermann-Kleiter et al., 2012). Briefly, *Nr2f6*$^{+/+}$ and *Nr2f6*-deficient $CD3^+$ T cells were isolated

untouched using the Pan T Cell Isolation Kit II mouse (Miltenyi Biotech, 130-090-861). $CD8^+$ T cells were isolated using either the mouse CD8 T Cell Isolation Kit II (Miltenyi Biotec, 130-104-075) or the human $CD8^+$ T Cell Isolation Kit (Miltenyi Biotec, 130-096-495). T cells were activated using plate-bound anti-CD3 (5µg/ml) and soluble anti-CD28 (1µg/ml) in complete IMDM medium. After activation, cells were harvested at the indicated time points and washed once in IMDM for subsequent fixation in 1% formaldehyde at 37°C for 10 min, and quenching of cross-linking by the addition of 1.375 M glycine. The cells were then washed twice with ice-cold PBS and lysed in cold cell lysis buffer for ChIP [5 mM PIPES (pH 8.0), 85 mM KCl, 0.5% Nonidet P-40 (NP-40)] for 10 min. After centrifugation, the cell pellets were lysed in 1 ml nuclei lysis buffer for ChIP [50 mM Tris-Cl (pH 8.0), 10 mM EDTA, 1% SDS] supplemented with protease inhibitors and incubated for 10 min on ice. After sonication with 25 30-s pulses using a Bioruptor Next Generation (Diagenode), the samples were centrifuged for 10 min at 12,000 rpm. The sheared chromatin was used to set up immunoprecipitation reactions with 5µg of the indicated antibodies (IgG, Santa Cruz sc-2027; NR2F6, R&D PP-N2025-00) at 4°C overnight. Magna ChIP protein G magnetic beads were added for 2h, and the samples were sequentially washed once with the buffers provided by the supplier (Imgenex; high to low salt). The DNA-protein complex was eluted by heating at 65°C overnight, and the DNA was eluted using the IPure kit (Diagenode). Real-time PCR was performed using an ABI PRIM 7000 Sequence Detection System (Applied Biosystems) with the following primers and probes: *Il2* minimal promoter (-380 – ATG): Forward: 5´ TTGTATGAATTAAAACTGCCACCTAAG 3´; Reverse: 5´CACTGACTGAATGGATTTAGGTGAA3´ with the probe 5´FAM-TTGGGCT AACCCGACCAAGAGGGA BHQ1-3 ´(Balasubramani et al., 2010). Distal *Il2* promoter (-1624): Forward: 5´ CAGTGTGCATGTAGCAGTCAA 3´; Reverse: 5´CACCACA CACCTACCCCATTT 3´; *Ifng* minimal promoter (-185): Forward: 5´ CGAGGAGCC TTCGATC AGGT 3´; Reverse: 5´GGTCAGCCGATGGCAGCTA 3´; with the probe 5´FAM TAAAACTGGAAGCCAGAGAGGTGCAGG- BHQ1-3´ (Balasubramani et al., 2010).

Flow cytometry. Splenocytes and lymph node cells were depleted of erythrocytes using the mouse erythrocyte lysing kit (R&D, WL2000) and mashed through a 100-µm filter. Splenocytes, lymph node cells, and TILs were incubated with FcR Block (BD Biosciences, 553142) to prevent nonspecific antibody binding before staining with appropriate surface antibodies for 30 min at 4°C, washed with PBS+2% FCS, and used for FACS analysis. For intracellular cytokine staining, cells were stimulated with 50 ng/ml Phorbol 12,13-dibutyrate (PDBu, Sigma, P1269), 500 ng ionomycin (Sigma, I0634) and GolgiPlug (BD Biosciences,

555029) for 4–5h. After fixation (cytokines: Biolegend fixation buffer (420801), 20 minutes, 4°C; transcription factors: FoxP3 staining buffer set (eBiosciences, 00-5523), >30 minutes, 4°C), cells were permeabilized with the fixation/permeabilization kit (BioLegend, 421002) for cytokines and the Foxp3-staining buffer set (eBiosciences, 00-5523) for transcription factors, incubated with FcR Block (BD Biosciences, 553142) before staining with specific cell surface or intracellular marker antibodies. Data acquisition was performed on a FACSCalibur or LSR Fortessa cell analyzer (Becton Dickinson). Data analysis was conducted using the Flowlogic software (eBioscience, version 1.6.0_35). The following antibodies were used for flow cytometry: CD4-V500 (BD, 560783), CD4-PE (BD, 553049), CD8a-APC (BD, 553035), CD25-PE (BD, 553866), CD11c-PE-Cy7 (BD, 558079), CD44-FITC (BD, 553270), CD62L-APC (BD, 553152), PD-1-PE (BD, 561788), Ki67-PE (BD, 556027), IL-17-PE (BD, 559502), IL-2-APC (BD, 554429), CD45-V500 (BD, 561487), CD11b-PE (BD, 557397), TNFa-PerCP Cy5.5 (BD, 560659), CD45-FITC (eBiosciences, 11-0451-82), CD8a-PerCP Cy5.5 (eBiosciences, 45-0081-82), DX-5-PE-Cy7 (eBiosciences, 25-5971-81), CD44-PerCP Cy5.5 (eBiosciences, 45-0441-82), TCR γδ-APC (eBiosciences, 17-5711-82), Foxp3-PE (eBiosciences, 12-4771-82), RORc (t)-APC (eBiosciences, 17-6988-82), GrzB-PerCP-710 (eBiosciences, 46-8898-82), IFNγ-PE-Cy7 (eBiosciences, 25-7311-82), MHCII-FITC (eBiosciences, 11-5321-82), Ly-6C-APC (eBiosciences, 17-5932-82), PDL-1-PerCP-eFluor710 (eBiosciences, 46-5982-80), CD45-APC (eBiosciences, 17-0451-81), CD3-PE-Cy7 (eBiosciences, 25-0031,82), FoxP3-FITC (eBiosciences, 11-5773-82), CD3-PE (eBiosciences, 12-0031-83), CD8a-bv421 (BioLegend, 100738), F4/80-PE-Cy7 (BioLegend, 123113), CD25-bv421 (BioLegend, 102034), Gr-1-FITC (BioLegend, 108405), F4/80-PE (BioLegend, 123109), CD11b-APC (BioLegend, 101211), Tbet-bv605 (BioLegend, 644817).

Gene expression analysis and MLPA. Total RNA was isolated using the RNeasy® Mini Kit (Quiagen). First-strand cDNA synthesis was performed using oligo(dT) primers (Promega) with the Qiagen Omniscript RT kit, according to the instructions of the supplier and as described previously (Hermann-Kleiter et al., 2012). Expression analysis was performed using real-time PCR with an ABI PRIM 7000 or ABI PRIM 7500fast Sequence Detection System with TaqMan gene expression assays (Applied Biosystems); all expression patterns were normalized to *Gapdh*. Multiplex Ligation-dependent Probe Amplification (MLPA) was performed using the SALSA® MLPA® EK1-RT kit purchased from MRC-Holland and used according to the manufacturer's instructions. Briefly, RNA was isolated, using the Quick-RNA™ MicroPrep (Zymo Research, #R1051) according to the manufacturer's instructions. Specific mRNAs were reversely transcribed into cDNA and bound by two oligonucleotides

consequently ligated by a heat stable ligase forming one probe. Each probe gives rise to an amplification product of unique length, separated by capillary sequencer (Genescan). Analysis was performed with GeneMapper (Applied Biosystems GmbH). The sum of all peak data was set to 100% to normalize for fluctuations between different samples, and single peaks were calculated relative to 100%. The following list of cell death related genes was quantified: BOK, SERPINB9, BCLW, BCLXL, FLIP, GUSB, BCL2, A1, MCL1, BAX, BAK, BCLG, BCLRAMBO, BID, BAD, BIK, BIM, BMF, BID3, MOAP1, APAF1, AIF, BCL2L10, XIAP, SURVIVIN, BIRC1A, BIRC7, CIAP1, CIAP2, NOXA, PUMA, BIRC6, OMI, B2M, TBP, P21, GZMB, PRF1, DIABLO, PAK2.

Treg and iTreg suppression assay. $CD25^+CD4^+$ and $CD25^-CD4^+$ T cells were isolated from spleens and LNs of *Nr2f6*$^{+/+}$ and *Nr2f6*$^{-/-}$ using the $CD4^+$ T cell isolation kit II followed by CD25-PE and anti-PE MicroBeads (all Miltenyi Biotec, 130-048-801) according to the manufacturer's recommendation. Sorted $CD25^-CD4^+$ T cells were labelled with 2.5µM CFSE (Molecular probes, C1157) for 4 min at 37°C; labelling was stopped by addition of fetal calf serum. T cell depleted splenocytes (using CD4 [130-049-201] and CD8a [130-049-401] MicroBeads, Miltenyi Biotec) treated for 45 min with 50µg/ml mitomycin C (AppliChem, A2190,0002) were used - after extensive washing - as APCs. To induce proliferation 0.5µg/ml antiCD3 (145-2C11, BioLegend) was added. $1x10^5$ CFSE-labeled $CD25^-CD4^+$ responder T cells were cultured with $1x10^5$ APCs in 96-well U-bottom tissue culture plates (Falcon). $CD25^+CD4^+$ T cells were added at the ratios 1+1, 1+4 and 1+9. To address suppression by iTregs *in vitro* differentiated iTregs were harvested at day 5 of culture (see below) and dead cells were removed using a dead cell removal kit (Miltenyi Biotec, 120-000-437) according to the manufacturer's recommendation. At day 3 of co-culture proliferation and activation (anti-CD25 staining) was analyzed by flow cytometry; 7-AAD or propidium iodide was added to exclude dead cells.

$CD4^+$ T cell differentiation cultures. Naïve $CD4^+$ T cells were isolated using the $CD4^+CD62L^+$ naïve T cell isolation kit II (Miltenyi Biotech, 130-093-227). Polarization of naïve $CD4^+$ T cells into iTregs was performed with 4µg/ml plate-bound anti-CD3 (clone: 2C11) and 1µg/ml anti-CD28 soluble in the presence of 5ng/ml recombinant mouse TGF-b and recombinant 20ng/ml hIL-2. Th1 polarization was performed with 5µg/ml anti-CD3 and 1µg/ml anti-CD28 in the presence of 10ng/ml mIL-12 and 5µg/ml anti-IL-4 (eBiosciences).

Gel mobility-shift assay. Electromobility assay was performed as described previously (Hermann-Kleiter et al., 2008).

Immunohistochemistry. Cryosections (5-7µm thickness) of TRAMP prostate or B16-OVA tumors from *Nr2f6*$^{+/+}$ and *Nr2f6*$^{-/-}$ mice were fixed and incubated with mouse monoclonal antibodies against the T cell markers CD4 and CD8 overnight at 4°C. Mouse monoclonal antibody anti-human CD4 (M731029, clone 4B12) and mouse monoclonal antibody anti-human CD8, (IS62330, clone C8/144B) were purchased from Dako. IHC analysis of TRAMP prostate and B16-OVA tumors were performed in triplicates of 4 biopsy specimens of *Nr2f6*$^{+/+}$ and *Nr2f6*$^{-/-}$ tumors. The sections were subsequently incubated with anti-mouse IgG Alexa Fluor 488® conjugate and Hoechst for 45 minutes at room temperature and mounted with Dako fluorescent mounting medium (S3023). Digital IHC images were acquired with an Axiovert 40 CFL (ZEISS) microscope.

Analysis of TCRVβ repertoire. Total RNA was prepared from *Nr2f6*$^{+/+}$ or *Nr2f6*$^{-/-}$ naïve or tumor draining inguinal lymph nodes as described in gene expression analysis. For TCRVβ analysis the TCRexpress™ Mouse Repertoire Clonality Detection Kit (BioMed Immunotech, M0561) was used in order to identify the Vβ gene families (from Vβ 1 to 20 with subfamilies Vβ 8.1, 8.2 and 8.3) of the CDR3 region according to the instructions of the supplier.

Statistics. Data were analyzed using Prism 5.03 software (GraphPad Software). Experiments were repeated at least two or three times. Data are represented as indicated (either the mean ± SEM or ± SD) for all figure panels in which error bars are shown. The P values were assessed using two-tailed unpaired student's t-test, log rank test, or ANOVA. A P value of less than 0.05 was considered statistically significant. *$p<0.05$; **$p<0.01$; ***$p<0.001$.

Supplemental References

Balasubramani, A., Shibata, Y., Crawford, G.E., Baldwin, A.S., Hatton, R.D., and Weaver, C.T. (2010). Modular utilization of distal cis-regulatory elements controls Ifng gene expression in T cells activated by distinct stimuli. Immunity 33, 35-47.

Carey, M.F., Peterson, C.L., and Smale, S.T. (2009). Chromatin immunoprecipitation (ChIP). Cold Spring Harbor protocols 2009, pdb prot5279.

Supplemental Figures and legends

Figure S1 related to Figure 1: Characterization of *Nr2f6*$^{+/+TRAMP}$ and *Nr2f6*$^{-/-TRAMP}$ TRAMP tumors and draining lymph nodes at week 22, 28 and endpoint.

Loss of NR2F6 in male TRAMP mice did not change the body weight of *Nr2f6*$^{+/+TRAMP}$ versus *Nr2f6*$^{-/-TRAMP}$ mice (A) at week 22, *Nr2f6*$^{+/+TRAMP}$ (n=9), *Nr2f6*$^{-/-TRAMP}$ (n=5), (B) at week 28, *Nr2f6*$^{+/+TRAMP}$ (n=19), *Nr2f6*$^{-/-TRAMP}$ (n=15) or at (C) endpoint analysis *Nr2f6*$^{+/+TRAMP}$ (n=4), *Nr2f6*$^{-/-TRAMP}$ (n=4). (D) *Nr2f6*-deficiency in male TRAMP mice correlates with higher numbers of TILs and T lymphocytes in dLN at week 28. Dot blots of CD45$^+$CD4$^+$ cells within the tumor dLN of *Nr2f6*$^{+/+TRAMP}$ and *Nr2f6*$^{-/-TRAMP}$ mice. Numbers adjacent to outlined areas indicate the percentage of positive cells relative to parental gate (CD45$^+$). (E) Bar charts depict percentages of CD4$^+$ cells (p=0.012), CD4$^+$CD44$^+$ cells (p=0.009), CD4$^+$INFγ^+ cells (p=0.006) within prostate tumor-draining lymph nodes of *Nr2f6*$^{+/+TRAMP}$ (n=7) and *Nr2f6*$^{-/-TRAMP}$ (n=11) mice are shown. (F) Dot blots of CD45$^+$CD8$^+$ cells within the tumor dLN of *Nr2f6*$^{+/+TRAMP}$ and *Nr2f6*$^{-/-TRAMP}$ mice. Numbers adjacent to outlined areas indicate the percentage of positive cells relative to parental gate (CD45$^+$). (G) Bar charts of total cell percentages within prostate tumor-draining lymph nodes, CD8$^+$ cells (p=0.004), CD8$^+$CD44$^+$ cells (p=0.017), and CD8$^+$INFγ^+ cells (p=0.03) of *Nr2f6*$^{+/+TRAMP}$ (n=7) and *Nr2f6*$^{-/-TRAMP}$ (n=11) mice are shown. (H) Percentages of CD45$^+$CD4$^+$RORc$^+$ as well as CD45$^+$TCR$\gamma\delta^+$ tumor infiltrating cells in *Nr2f6*$^{+/+TRAMP}$ (n=11), *Nr2f6*$^{-/-TRAMP}$ (n=7) mice were increased at week 28, which however did not reach statistical significance. (I) In prostate tumor dLN a tendency towards more CD45$^+$ CD4$^+$IL-17$^+$, CD8$^+$T-bet$^+$, DX5$^+$, and TCR$\gamma\delta^+$ cells could be detected in *Nr2f6*$^{-/-TRAMP}$ (n=7) when compared to *Nr2f6*$^{+/+TRAMP}$ (n=11) mice. (J) Loss of NR2F6 in male TRAMP mice correlates with higher numbers of TILs and cytokine secreting T lymphocytes in dLN at week 22. Gross examination of UG tracts at week 22 from *Nr2f6*$^{+/+TRAMP}$ (n=9) and *Nr2f6*$^{-/-TRAMP}$ (n=5) mice shows decreased UG tract size in *Nr2f6*$^{-/-TRAMP}$ mice. (K) Prostate weight (p=0.003) as well as the ratio between UG tract and body weight (p=0.002) was significantly decreased in *Nr2f6*$^{-/-TRAMP}$ mice. (L) Higher numbers of CD45$^+$ tumor infiltrating lymphocytes (p=0.006) as well as (M) tumor draining lymph node cells, especially CD4$^+$IL-2$^+$ T cells (p=0.007) could be detected in *Nr2f6*$^{-/-TRAMP}$ (n=5) mice when compared to cells isolated from *Nr2f6*$^{+/+TRAMP}$ (n=9) mice, bar charts and representative dot blots are shown. Numbers adjacent to outlined areas indicate percentages of cells within the gates. Results shown are derived from at least two independent experiments. Error bars represent the mean ± SEM.

Figure S2 related to Figure 2: TCRVβ repertoire in naïve and B16-OVA tumor draining lymph nodes of *Nr2f6*$^{+/+}$ and *Nr2f6*$^{-/-}$ mice is not altered.

TCRVβ repertoire of (A) wild-type and (B) *Nr2f6*-deficient T lymphocytes within naive or tumor draining lymph (dLN) nodes was investigated via clonality analysis of the 22 individual Vβ gene families (from Vβ 1 to 20 with subfamilies Vβ 8.1, 8.2 and 8.3) of the CDR3 region. Nested PCR products were separated on a high resolution agarose gel. Data shown are representatives of two independent experiments as well as negative (-) & positive controls (+) are given.

Figure S3 related to Figure 3: Increased numbers of tumor infiltrating T cells in *Nr2f6*-deficient mice bearing B16-OVA transplantable melanomas.

(A) Representative dot plots of tumor infiltrating $CD8^+$ and $CD4^+$ cells gated on $CD45^+$ derived from *Nr2f6*$^{+/+}$ and *Nr2f6*$^{-/-}$ mice. (B) A representative analysis of the flow cytometric gating strategy for discerning tumor infiltrating immune cells is depicted, whereby gated populations (from left to right) are indicated defining forward and side scatter, doublets, $CD45^+CD3^+CD4^+CD8^+$ and as one further example $CD45^+CD3^+CD8^+PD\text{-}1^+$ populations. (C) Tumor immune cell infiltration rate is not dependent on tumor size but differs in general, $CD45^+$ and $CD3^+$ parental cell percentages in small [up to 0.021g; maximum 52.5mm^3], medium [0.022g – 0.111g; maximum 271mm^3] and large [0.112g – 0.370g; maximum 845mm^3] tumors of *Nr2f6*$^{+/+}$ or *Nr2f6*$^{-/-}$ mice are shown by dot blots. (D) Representative cryosections of B16-OVA melanomas from *Nr2f6*$^{+/+}$ or *Nr2f6*$^{-/-}$ mice stained for the T cell markers CD4 and CD8 in green and Hoechst nuclear stain in blue. Scale bar=50µm. (E) Graphical representation of enhanced $CD4^+$ ($p=0.003$), and $CD8^+$ ($p=0.003$) tumor T cell infiltration in *Nr2f6*$^{-/-}$ mice, averaged from three fields per mouse and four mice per genotype. (F) Immune cell numbers and characterization of *Nr2f6*$^{+/+}$ (n=6) and *Nr2f6*$^{-/-}$ (n=7) B16-OVA tumor infiltrating cells analyzed by the following markers and gates: $CD45^+$ ($p=0.0003$), $CD45^+CD3^+$ ($p=0.0002$), $CD45^+CD8^+$ ($p=0.01$), and $CD45^+CD4^+$ ($p=0.005$), as also shown by dot blots in Figure S3A. Error bars represent ± SEM, differences were analyzed using student's t-test.

Figure S4 related to Figure 4: *Nr2f6* expression impairs expression of IL-2 and IFNγ as well as activation markers within the tumor draining lymph nodes.

Analysis of B16-OVA tumor-draining lymph nodes from *Nr2f6*$^{+/+}$ and *Nr2f6*$^{-/-}$ mice on day 14 are shown. (A) Dot blots of enhanced CD45^{+}CD4^{+} cell numbers in *Nr2f6*$^{-/-}$ dLN. (B) Bar charts of dLN cell percentages of CD4^{+} (p=0.04) , CD4^{+}IL-2^{+} (p=0.01), and total CD4^{+}IFNγ^{+} (p=0.006) cells as well as (C) CD8^{+} (p=0.004), CD8^{+}IL-2^{+} (p=0.007) and total CD8^{+}IFNγ^{+} (p=0.03) cells. Numbers indicate % of cells within the gates, and the results shown are derived from at least two independent experiments. (D) Enhanced numbers of activated CD44^{+} tumor infiltrating CD4^{+} (p=0.009) and CD8^{+} (p=0.017) cells were detected in *Nr2f6*$^{-/-}$ (n=8) compared to *Nr2f6*$^{+/+}$ (n=8) mice, whereas no differences were observed for (E) NK (based on the marker DX5^{+}), macrophages (CD11b^{+}) or DC subsets (CD11c^{+} CD11b^{+} and CD11c^{+}CD8a^{+}). Data are shown by bar charts and error bars represent ± SEM, data were analyzed via student's t-test.

Figure S5 related to Figure 5: T cell status of healthy mice and gross examination of tumor growth in *Rag1*$^{-/-}$ mice reconstituted with either CD3$^{Nr2f6+/+}$ or CD3$^{Nr2f6-/-}$ T cells.

(A) Single cell suspension of an inguinal lymph node derived from 13-16 week old female *Nr2f6*$^{+/+}$ (n=7) or *Nr2f6*$^{-/-}$ (n=7) mice was analyzed by flow cytometry (3 independent experiments, statistics student´s t-test). (B) Gross examination of tumor growth in *Rag1*-deficient mice reconstituted with either CD3$^{Nr2f6+/+}$ or CD3$^{Nr2f6-/-}$ 14 days before subcutaneous inoculation with 1.5×10^{5} EG7 cells. Pictures of tumors were taken at the indicated time points of *Rag1*$^{-/-}$ PBS, *Rag1*$^{-/-}$CD3$^{Nr2f6+/+}$ and *Rag1*$^{-/-}$CD3$^{Nr2f6-/-}$ mice, asterisk depicts representative a picture of another *Rag1*$^{-/-}$CD3$^{Nr2f6-/-}$ mouse. (C) Flow cytometric analysis revealed increased CD4^{+} T cell numbers in the dLNs of tumor bearing *Rag*1$^{-/-}$CD3$^{Nr2f6-/-}$ mice (p=0.03) when compared to tumor dLNs of *Rag*1$^{-/-}$CD3$^{Nr2f6+/+}$ mice.

Figure S6 related to Figure 6: *Nr2f6* does neither influence nTreg & iTreg numbers and their suppressive capacity nor cell survival.

(A) Representative CFSE profiles of *Nr2f6*$^{+/+}$CD25^{-}CD4^{+} T cells either non-stimulated (-) or stimulated with anti-CD3 antibodies and mitomycin-treated APCs (+) for 3 days - without or with CD25^{high}CD4^{+} Treg cells isolated from either *Nr2f6*$^{+/+}$ or *Nr2f6*$^{-/-}$ mice at a ratio of 1:4. The frequency of divided cells is included in each histogram. (B) Proliferation of CFSE-labeled CD25^{-}CD4^{+} T cells is depicted as % of dividing cells (in bar charts). Results (mean ± SD) of two independent experiments performed in duplicates are shown. (C) Frequency of Foxp3^{+}CD25^{+} cells in peripheral LN of *Nr2f6*$^{+/+}$ or *Nr2f6*$^{-/-}$ mice was analyzed by flow cytometry. Representative dot plots (gated on CD45^{+}CD3^{+}CD4^{+}) are shown. (D) *In vitro* differentiated *Nr2f6*$^{+/+}$ or *Nr2f6*$^{-/-}$ iTreg cells (at day 5 of culture) were analyzed for their suppressive capacity using *in vitro* co-cultures. Proliferation of CFSE-labeled CD25^{-}CD4^{+} T cells (*Nr2f6*$^{+/+}$) is depicted as percent dividing cells (in bar charts) of either non-stimulated (-) or anti-CD3 antibody and mitomycin-treated APC stimulated (+) for 3 days – and in the presence of iTreg cells from either *Nr2f6*$^{+/+}$ or *Nr2f6*$^{-/-}$ mice at a ratio of 1:1. Results of 2 independent experiments each performed with T cells isolated from two individual mice (duplicates per mouse) are shown (n =4). (E) *In vitro* qRT-PCR analysis of *Foxp3* expression in CD4^{+} *Nr2f6*$^{+/+}$ cells compared to *Nr2f6*$^{-/-}$ cells during iTreg differentiation (5µg anti-CD3; 1µg anti-CD28 supplemented with 5ng/ml TGFβ and 20ng/ml IL-2) at the indicated time points (n=3). Expression was normalized to the house-keeping gene GAPDH and presented as fold induction of unstimulated control cells. Summary graphs are mean ± SD, and data are representative of at least two independent experiments, statistics were analyzed by two-way ANOVA. (F) *In vitro* differentiated iTreg cells (at day 5 of culture) were analyzed for the frequency of Foxp3^{+}CD25^{+} by flow cytometry (n=4). (G) CD4^{+} T cells were FACS-sorted from *Nr2f6*$^{+/+}$ and *Nr2f6*$^{-/-}$ spleens, RNA was isolated and RT-MLPA was performed assessing relative mRNA abundances of 42 different proteins associated with cell death (n=4, statistics: two-way ANOVA and Bonferroni post-tests). Note that gene expression with apparently different expression between genotypes was subsequently re-evaluated by qRT-PCR – no significant differences could be detected (n=4, statistics: two-way ANOVA and Bonferroni post-tests).

Figure S7 related to Figure 7: *Nr2f6* suppresses *Il2* and *Ifng* expression in CD8$^+$ T cells but not viability or apoptosis.

(A) CD8$^+$ *Nr2f6*$^{+/+}$ or *Nr2f6*$^{-/-}$ cells were activated *in vitro* with anti-CD3 (5µg) and anti-CD28 (1µg) over time (d2, d3), followed by a re-stimulation with anti-CD3 (5µg) over night (d4/re), IL-2 and IFNγ expression was analyzed via flow cytometry. Numbers within outlined areas indicate percentage of positive cells. One out of three representative experiments is shown. (B) CD8$^+$ T cells were FACS-sorted from *Nr2f6*$^{+/+}$ and *Nr2f6*$^{-/-}$ spleens, RNA was isolated and RT-MLPA was performed assessing relative mRNA abundances of 42 different proteins associated. Note that gene expression with apparently different expression between genotypes was subsequently re-evaluated by qRT-PCR – no significant differences could be detected (n=4, statistics: 2-way Anova and Bonferroni post-tests). (C) *Nr2f6*$^{+/+}$ and *Nr2f6*$^{-/-}$ CD8$^+$ T cells were activated with anti-CD3 (0.5µg or 5µg) and anti-CD28 (1µg) for 20h *in vitro*, nuclear extracts were isolated and EMSA loading amounts were controlled by performing western blots with nuclear extracts probed with lamin B. No gross differences could be observed between the genotypes using the described conditions. One out of two representative experiments is shown. (D) ChIP PCR of resting or 20h anti-CD3 (0.5µg or 5µg) and anti-CD28 (1µg) activated CD3$^+$ T cells for minimal *Il2* promoter, (E) distal (-1.4kb) *Il2* promoter or (F) minimal *Ifng* promoter, respectively. Chromatin was immunoprecipitated with anti-NR2F6, anti-NFAT2 or IgG control, and promoter sequences were quantified by real time PCR. One representative independent experiment out of two is shown.

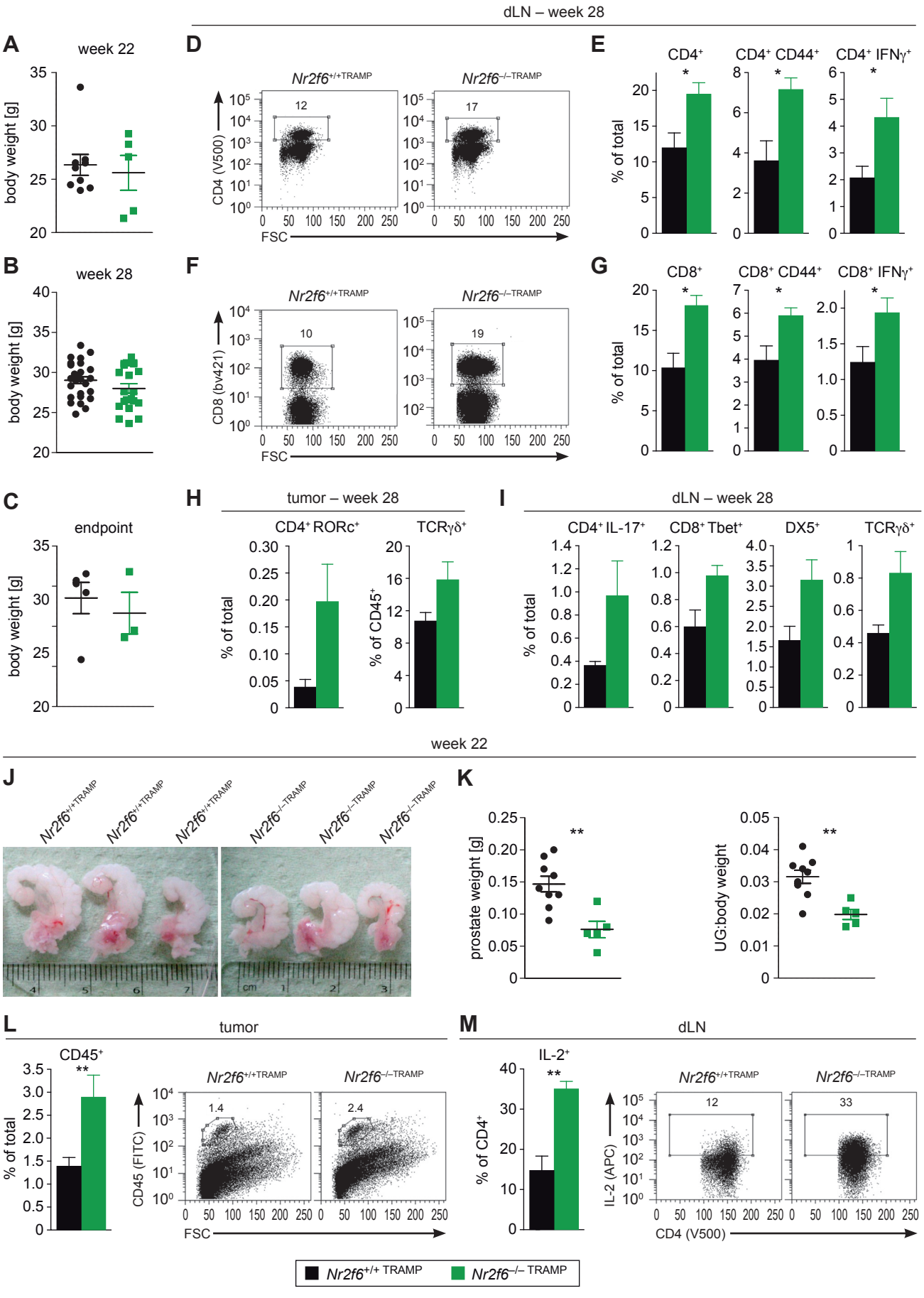
dLN – week 28
A
week 22
body weight [g]
B
week 28
C
endpoint
D
Nr2f6+/+TRAMP
Nr2f6−/−TRAMP
CD4 (V500)
FSC
E
CD4+
CD4+ CD44+
CD4+ IFNγ+
% of total
F
CD8 (bv421)
G
CD8+
CD8+ CD44+
CD8+ IFNγ+
H
tumor – week 28
CD4+ RORc+
TCRγδ+
% of CD45+
I
dLN – week 28
CD4+ IL-17+
CD8+ Tbet+
DX5+
week 22
J
K
prostate weight [g]
UG:body weight
L
tumor
CD45+
CD45 (FITC)
M
dLN
IL-2+
% of CD4+
IL-2 (APC)
Nr2f6+/+ TRAMP
Nr2f6−/− TRAMP

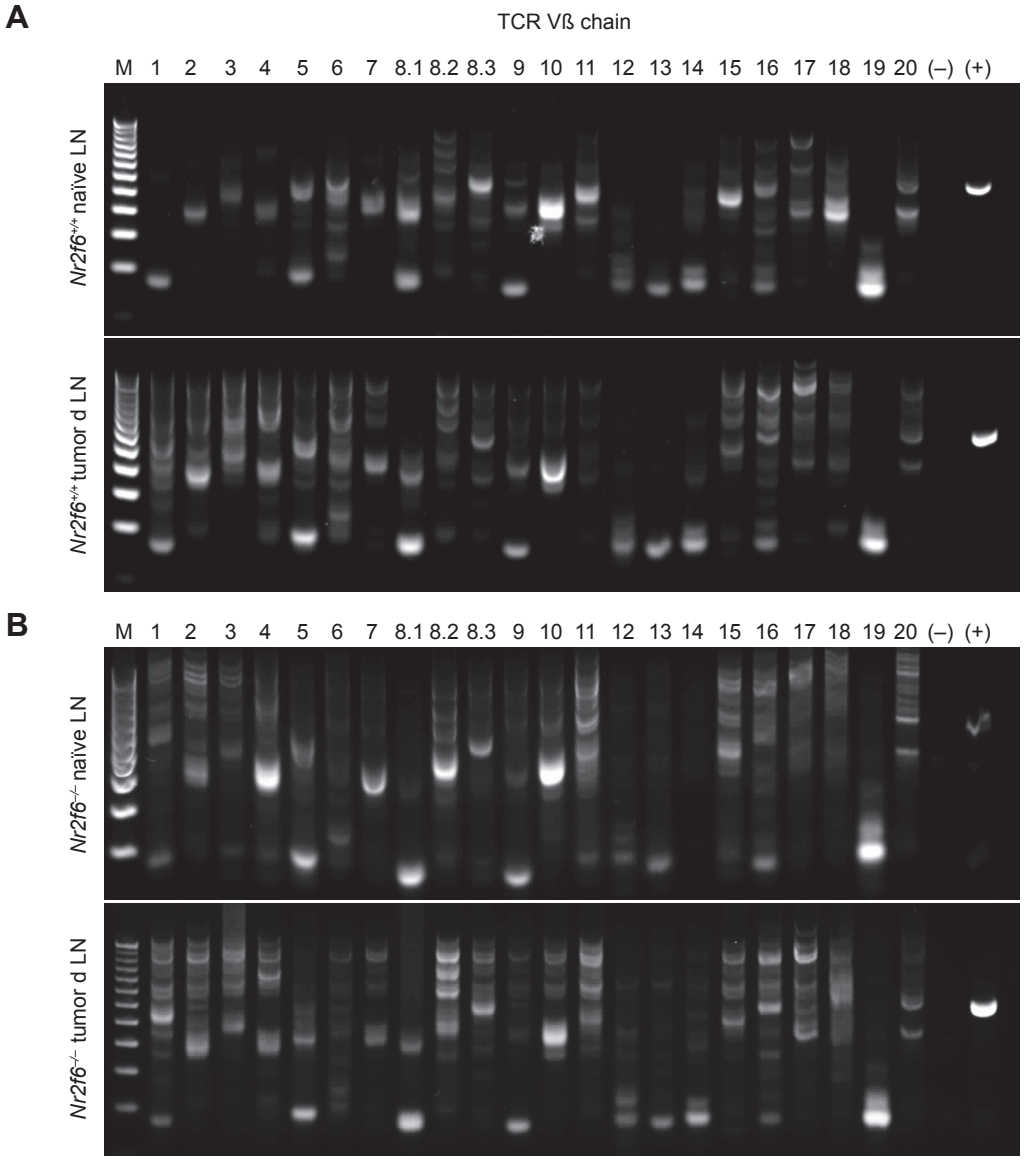
A
TCR Vß chain
M 1 2 3 4 5 6 7 8.1 8.2 8.3 9 10 11 12 13 14 15 16 17 18 19 20 (–) (+)
Nr2f6+/+ naïve LN
Nr2f6+/+ tumor d LN
B
M 1 2 3 4 5 6 7 8.1 8.2 8.3 9 10 11 12 13 14 15 16 17 18 19 20 (–) (+)
Nr2f6−/− naïve LN
Nr2f6−/− tumor d LN

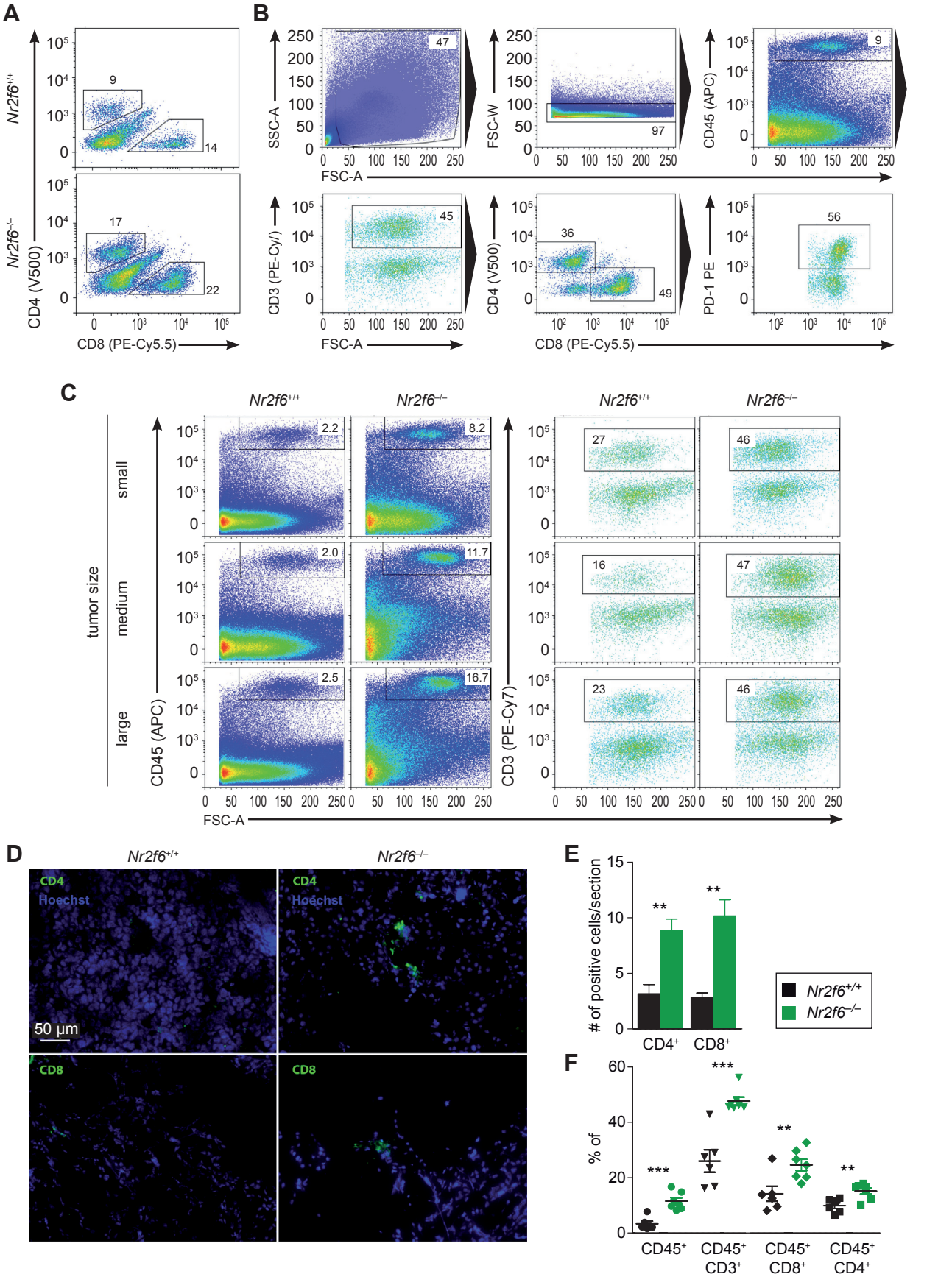
A
B
C
D
E
F
Nr2f6+/+
Nr2f6−/−
CD4 (V500)
CD8 (PE-Cy5.5)
SSC-A
FSC-A
FSC-W
CD45 (APC)
CD3 (PE-Cy/)
PD-1 PE
tumor size
small
medium
large
CD3 (PE-Cy7)
CD4
Hoechst
CD8
50 µm
# of positive cells/section
CD4+
CD8+
% of
CD45+
CD45+ CD3+
CD45+ CD8+
CD45+ CD4+

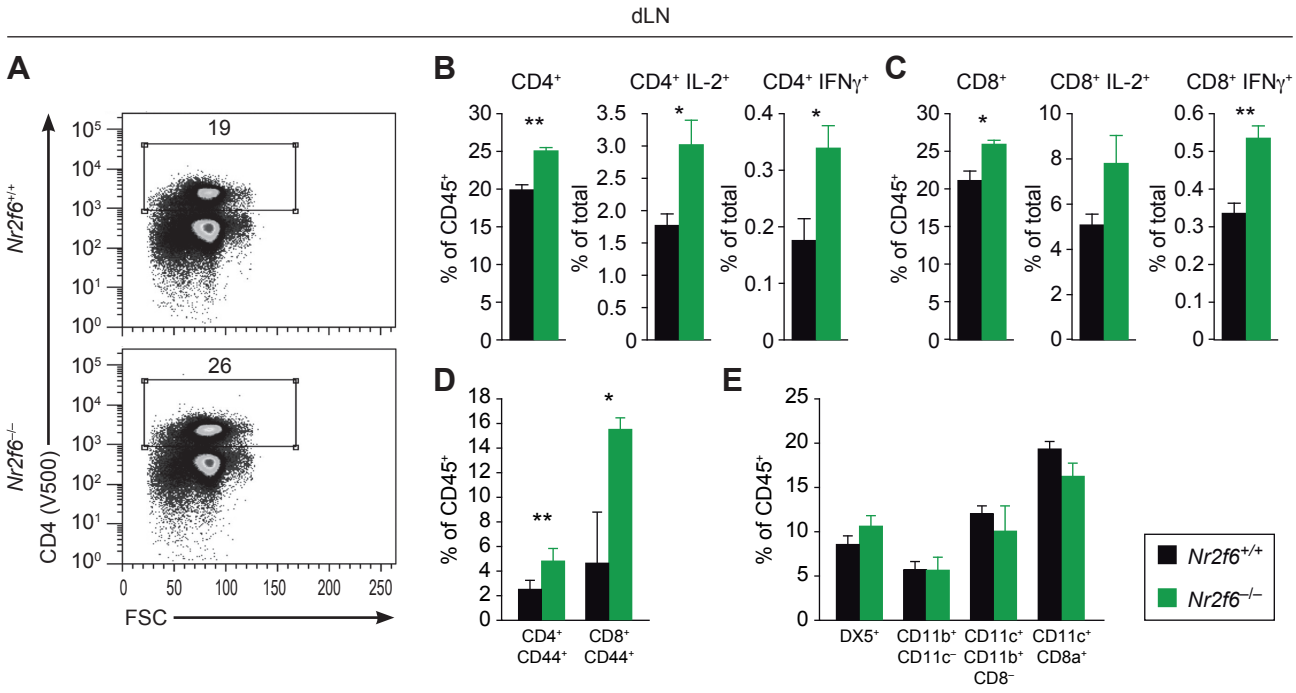
dLN
A
Nr2f6+/+
Nr2f6−/−
CD4 (V500)
FSC
19
26
B
CD4+
CD4+ IL-2+
CD4+ IFNγ+
% of CD45+
% of total
C
CD8+
CD8+ IL-2+
CD8+ IFNγ+
D
CD4+ CD44+
CD8+ CD44+
E
DX5+
CD11b+ CD11c−
CD11c+ CD11b+ CD8−
CD11c+ CD8a+
Nr2f6+/+
Nr2f6−/−

A. T cell status in healthy Nr2f6$^{+/+}$ and Nr2f6$^{-/-}$ lymph nodes (all numbers)

	***Nr2f6*$^{+/+}$**	***Nr2f6*$^{-/-}$**	p values
Total (x 10^5)	38 ± 21	35 ± 25	0.79
T cells			
CD3$^+$	18 ± 14	16 ± 11	0.85
CD3$^+$CD4$^+$	9.1 ± 7	9.4 ± 6	0.93
CD4$^+$CD25$^+$Foxp3$^+$	1.1 ± 0.8	1.1 ± 0.8	0.93
CD4$^+$CD25$^+$	6.1 ± 4.3	6.1 ± 4	0.39
CD3$^+$CD8$^+$	7.6 ± 6	6.2 ± 4.7	0.65
CD8$^+$CD25$^+$	3.2 ± 2.6	2.4 ± 2	0.56
Cytokines (4h PDBu/Ionomycin re-stimulated)			
CD4$^+$IL-2	1.6 ± 1	1.5 ± 1.2	0.91
CD4$^+$IFNγ	1.7 ± 0.7	1.7 ± 1	1.0
CD4$^+$TNFα	3.2 ± 1.9	4.1 ± 2.8	0.52
CD8$^+$IL-2	1.1 ± 0.6	0.6 ± 0.6	0.26
CD8$^+$IFNγ	1.9 ± 1.2	1.5 ± 0.9	0.53
CD8$^+$TNFα	2.5 ± 1.5	1.8 ± 1.1	0.40

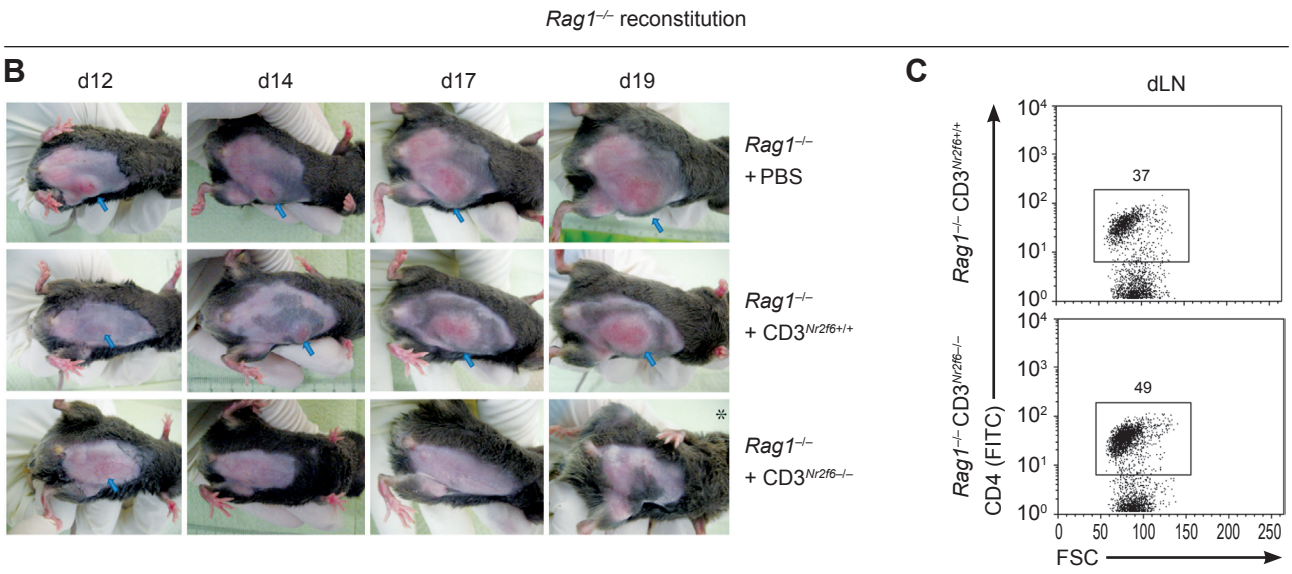

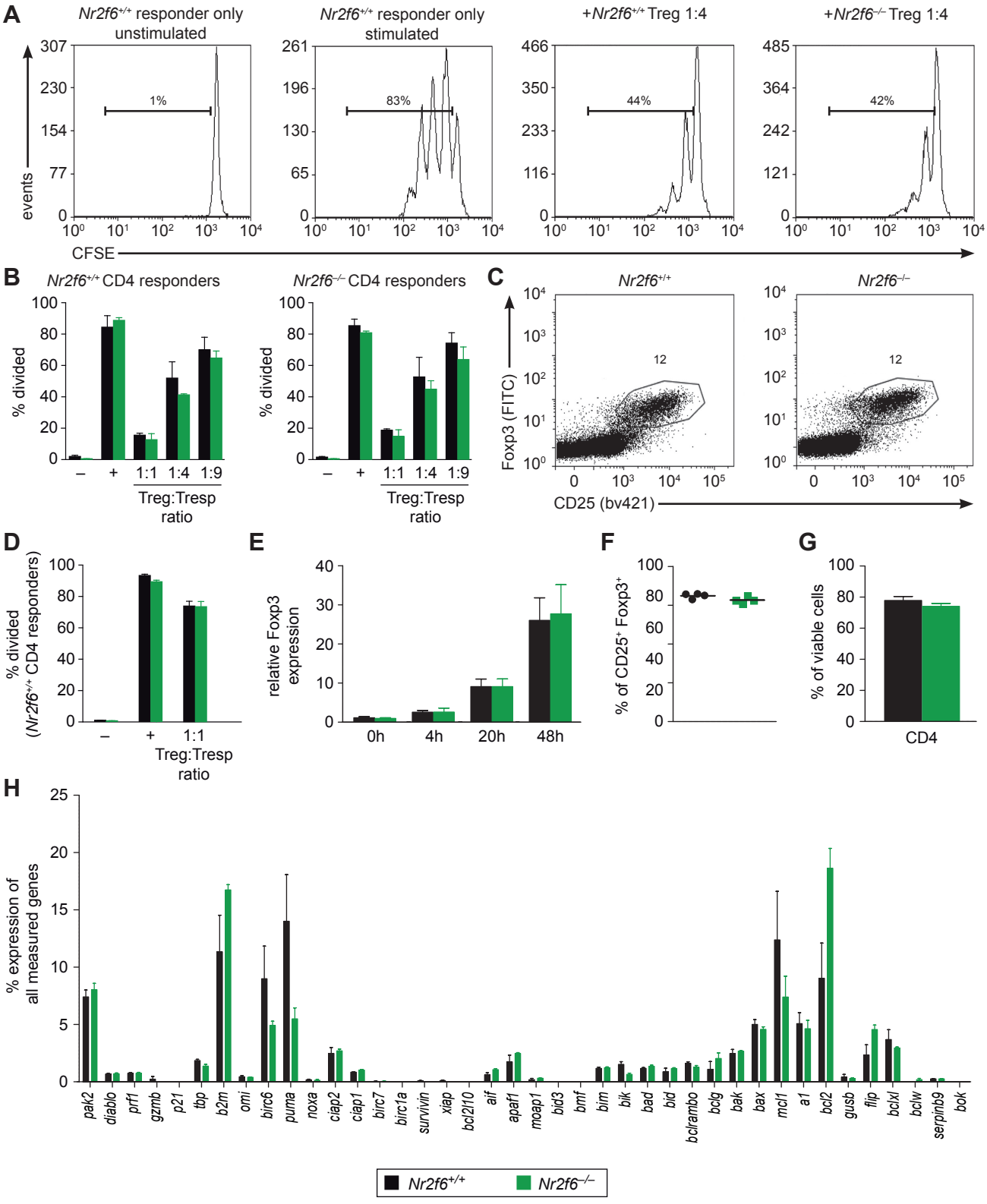
A
Nr2f6+/+ responder only unstimulated
Nr2f6+/+ responder only stimulated
+Nr2f6+/+ Treg 1:4
+Nr2f6−/− Treg 1:4
1%
83%
44%
42%
events
CFSE
B
Nr2f6+/+ CD4 responders
Nr2f6−/− CD4 responders
% divided
– + 1:1 1:4 1:9
Treg:Tresp ratio
C
Nr2f6+/+
Nr2f6−/−
12
Foxp3 (FITC)
CD25 (bv421)
D
% divided (Nr2f6+/+ CD4 responders)
– + 1:1
Treg:Tresp ratio
E
relative Foxp3 expression
0h 4h 20h 48h
F
% of CD25+ Foxp3+
G
% of viable cells
CD4
H
% expression of all measured genes
pak2 diablo prf1 gzmb p21 tbp b2m omi birc6 puma noxa ciap2 ciap1 birc7 birc1a survivin xiap bcl2l10 aif apaf1 moap1 bid3 bmf bim bik bad bid bclrambo bclg bak bax mcl1 a1 bcl2 gusb flip bclxl bclw serpinb9 bok
Nr2f6+/+
Nr2f6−/−

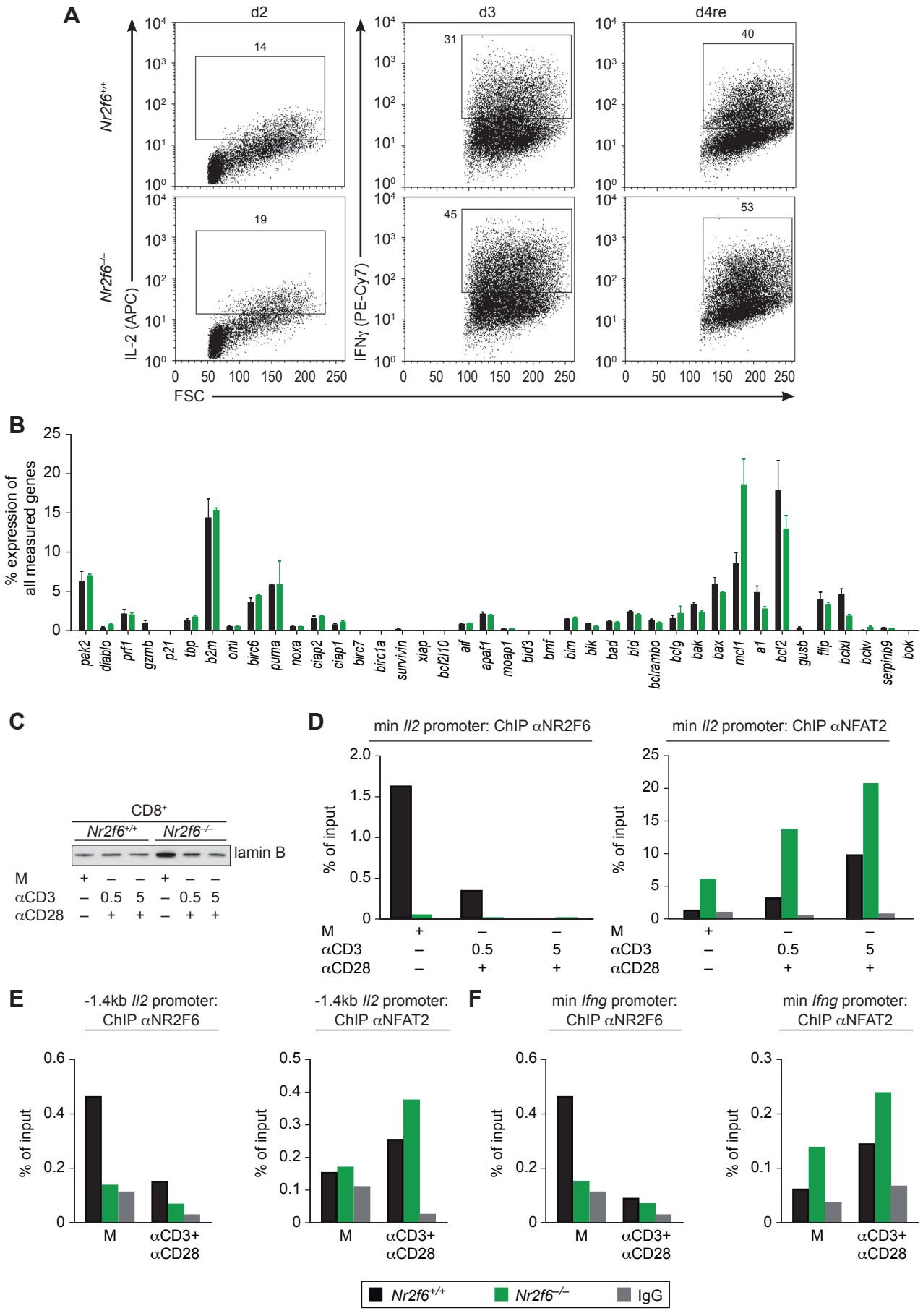
A
d2
d3
d4re
Nr2f6+/+
Nr2f6−/−
IL-2 (APC)
IFNγ (PE-Cy7)
FSC
14
19
31
45
40
53
B
% expression of all measured genes
pak2 diablo prf1 gzmb p21 tbp b2m omi birc6 puma noxa ciap2 ciap1 birc7 birc1a survivin xiap bcl2l10 aif apaf1 moap1 bid3 bmf bim bik bad bid bclrambo bclg bak bax mcl1 a1 bcl2 gusb flip bclxl bclw serpinb9 bok
C
CD8+
Nr2f6+/+
Nr2f6−/−
lamin B
M + – – + – –
αCD3 – 0.5 5 – 0.5 5
αCD28 – + + – + +
D
min Il2 promoter: ChIP αNR2F6
min Il2 promoter: ChIP αNFAT2
% of input
M + – –
αCD3 – 0.5 5
αCD28 – + +
E
-1.4kb Il2 promoter: ChIP αNR2F6
-1.4kb Il2 promoter: ChIP αNFAT2
F
min Ifng promoter: ChIP αNR2F6
min Ifng promoter: ChIP αNFAT2
M
αCD3+ αCD28
Nr2f6+/+
Nr2f6−/−
IgG